

A higher order nonconforming virtual element method for the Cahn-Hilliard equation

Andreas Dedner* and Alice Hodson†

Abstract

In this paper we develop a fully nonconforming virtual element method (VEM) of arbitrary approximation order for the two dimensional Cahn-Hilliard equation. We carry out the error analysis for the semidiscrete (continuous-in-time) scheme and verify the theoretical convergence result via numerical experiments. We present a fully discrete scheme which uses a convex splitting Runge-Kutta method to discretize in the temporal variable alongside the virtual element spatial discretization.

Keywords: virtual element method, Cahn-Hilliard equation, nonlinear, fourth-order problems, nonconforming, DUNE.

1 Introduction

Let $\Omega \subset \mathbb{R}^2$ denote a polygonal domain, with boundary $\partial\Omega$ and outward pointing normal n . Originally introduced by Cahn and Hilliard in [14, 15] to model the phase separation of a binary alloy, we consider the following two dimensional Cahn-Hilliard problem: find $u(x, t) : \Omega \times [0, T] \rightarrow \mathbb{R}$ such that

$$\partial_t u - \Delta(\phi(u) - \varepsilon^2 \Delta u) = 0 \quad \text{in } \Omega \times (0, T], \quad (1.1a)$$

$$u(\cdot, 0) = u_0(\cdot) \quad \text{in } \Omega, \quad (1.1b)$$

$$\partial_n u = 0, \partial_n(\phi(u) - \varepsilon^2 \Delta u) = 0 \quad \text{on } \partial\Omega \times (0, T], \quad (1.1c)$$

for time $T > 0$. We use the notation ∂_n for denoting the normal derivative and $\varepsilon > 0$ to represent the interface parameter. We define $\phi(x) = \psi'(x)$, where the free energy $\psi : \mathbb{R} \rightarrow \mathbb{R}$ is defined as

$$\psi(x) := \frac{1}{4}(1 - x^2)^2. \quad (1.2)$$

As described in [14, 15, 27], phase separation is a physical phenomenon occurring when a high temperature mixture is cooled down quickly and the two or more components in the mixture separate into regions of each one. As well as being used as a model for this type of phenomena, Cahn-Hilliard type equations have been used in a wide range of problems such as image processing [26], for example. Due to the numerous applications of the Cahn-Hilliard equation, there has been a lot of attention and research dedicated to numerical methods for this problem.

Many classical methods used to solve the Cahn-Hilliard equation have been finite element (FE) based methods. These approaches can be split into two types. In the first, the equations are reformulated in mixed form, resulting in a system of second order problems which can be solved using classical methods suitable for elliptic problems, e.g., [30, 37]. The second approach involves solving the equations directly in their weak form, requiring the use of second order derivatives of the finite element functions. Solving the variational formulation of the fourth-order problem directly using FE methods is not straightforward due to the higher regularity requirements which have to be imposed on the finite element basis functions. Fully conforming methods [28, 31] require a large number of degrees of freedom even for the lowest order approximation or are based on sub triangulation. An easier approach is based on using suitable nonconforming spaces and to possibly include stabilization terms to achieve stability [18, 45]. A few nonconforming spaces have been suggested which have sufficient regularity to be stable without extra penalty terms [29, 47]. However, higher order versions of these spaces are not easily obtained. Consequently, there are few methods for fourth-order problems readily available in software packages, with most only providing the lowest order Morley element for these types of problems.

More recently, we have seen a handful of virtual element methods to discretize the Cahn-Hilliard equation [3, 39, 40]. The virtual element method is an extension and generalization of both finite element and mimetic

*Department of Mathematics, University of Warwick, Coventry, CV4 7AL, UK. Email: a.s.dedner@warwick.ac.uk

†Corresponding author. Department of Numerical Mathematics, Charles University, Sokolovská 83, 186 75 Praha 8, Czech Republic. Email: hodson@karlin.mff.cuni.cz

difference methods. First introduced for second order elliptic problems in [8], virtual elements are highly desirable due to the straightforward way in which they extend to general polygonal meshes. The virtual element method is incredibly versatile and as such has been applied to a wide range of problems; for example, the development of higher order continuity spaces [11] suitable for e.g. the approximation of polyharmonic problems [5] as well as the construction of pointwise divergence-free spaces for the Stokes problem [10]. Other methods which have been considered for the discretization of problem (1.1) include the hybrid high-order (HHO) method (see [25] where the method was first introduced for a linear elasticity problem) as well as isogeometric analysis [35, 36]. In [17] an HHO approximation of the Cahn-Hilliard equation in mixed form is considered and, like the VEM approach, extends easily to general polygonal meshes.

A VEM discretization for problem (1.1) is considered in [3] where a C^1 -conforming method is presented with only 3 degrees of freedom (dof) per vertex. Another conforming approach is considered in [39] however the problem is formulated in mixed form. Both works present a semidiscrete (continuous-in-time) convergence result for the lowest order VEM space. The only other applications of the virtual element method to the Cahn-Hilliard equation are seen in the following two works. In [40] a fully discrete scheme is presented and is shown to satisfy both a discrete energy law and a mass conservation law. A numerical exploration of Cahn-Hilliard type equations is presented in [6]. In contrast to the virtual element discretizations developed in [3, 39, 40], we present the first analysis of a higher order VEM method and achieve optimal order error estimates for the semidiscrete scheme. A clear advantage of using higher order methods is the ability to use considerably lower grid resolutions which in turn can avoid the use of strongly adapted grids.

The aim of this paper is to present a new nonconforming virtual element method for the discretization of the Cahn-Hilliard equation. Our approach for constructing the VEM space follows [21]. We show that by defining the projection operators without using the underlying variational problem, we can directly apply our method to nonlinear fourth-order problems. Consequently, our approach does not require any special treatment of the nonlinearity as in [3]. Our method is shown to converge with optimal order also in the higher order setting. This projection approach has been implemented within the DUNE software framework [7, 23] requiring little change to the existing code base. To the best of our knowledge, this is the first analysis of a nonconforming virtual element method for the Cahn-Hilliard equation as well as the only higher order method without using a mixed formulation of (1.1).

This paper is organized in the following way. In Section 2 we introduce the weak form of the continuous fourth-order Cahn-Hilliard problem, followed by the virtual element method discretization in Section 3. In Section 4 we carry out the error analysis of the continuous-in-time scheme before presenting numerical experiments to verify the theoretical results in Section 5. Finally, we give proofs of some technical lemmas in Appendix A.

2 Problem formulation

We begin by introducing the variational formulation of problem (1.1) before introducing notation and some technicalities needed for the rest of the paper.

2.1 The continuous problem

First, we introduce the following space

$$V = \{v \in H^2(\Omega) : \partial_n v = 0 \text{ on } \partial\Omega\}.$$

Then, the variational form for (1.1) is described as follows: for a.e. $t \in (0, T)$ find $u(\cdot, t) \in V$ such that

$$\begin{aligned} (\partial_t u, v) + \varepsilon^2 a(u, v) + r(u; u, v) &= 0 \quad \forall v \in V \\ u(\cdot, 0) &= u_0(\cdot) \in V \end{aligned} \tag{2.1}$$

where the bilinear form $a(\cdot, \cdot)$ is the standard hessian form arising in the study of fourth-order problems

$$a(v, w) = (D^2 v, D^2 w) = \int_{\Omega} (D^2 v) : (D^2 w) \, dx = \int_{\Omega} \sum_{i,j=1}^2 \frac{\partial^2 v}{\partial x_i \partial x_j} \frac{\partial^2 w}{\partial x_i \partial x_j} \, dx,$$

and the semilinear form $r(\cdot; \cdot, \cdot)$ is defined as

$$r(z; v, w) = \int_{\Omega} \phi'(z) Dv \cdot Dw \, dx$$

for all $z, v, w \in V$. Existence and uniqueness of a solution u to problem (2.1) where $u \in L^\infty(0, T; V) \cap L^2(0, T; H^4(\Omega))$, and $u_t \in L^2(0, T; L^2(\Omega))$ can be found in e.g. [29]. Further, higher regularity of u_t can be derived, provided that $-\Delta^2 u_0 + \Delta \phi(u_0) \in V$ (see e.g. [31]).

Note that we can view the Cahn-Hilliard equation as the H^{-1} gradient flow of the following free energy functional

$$E(u) = \int_{\Omega} \left(\psi(u) + \frac{\varepsilon^2}{2} |\nabla u|^2 \right) \, dx, \tag{2.2}$$

and notice that the total energy $E(u)$ decreases with time, $\frac{d}{dt}E(u(t)) \leq 0$.

2.2 Basic spaces and notation

Throughout this paper we use the notation $a \lesssim b$ to mean that $a \leq Cb$ for some constant C , which does not depend on h .

We denote the space of polynomials of degree less than or equal to ℓ on a set $K \subseteq \mathbb{R}^2$ by $\mathbb{P}_\ell(K)$. We denote a decomposition of the space Ω by \mathcal{T}_h and let h_K denote the diameter of a polygon $K \in \mathcal{T}_h$ where $\text{diam}(K) = \max_{x,y \in K} \|x - y\|$. We will denote the edges of a polygon $K \in \mathcal{T}_h$ by $e \subset \partial K$ and denote the set of all edges in \mathcal{T}_h by $\mathcal{E}_h = \mathcal{E}_h^{\text{int}} \cup \mathcal{E}_h^{\text{bdry}}$, split into boundary and internal edges respectively. Similarly, denote the set of vertices in \mathcal{T}_h by $\mathcal{V}_h = \mathcal{V}_h^{\text{int}} \cup \mathcal{V}_h^{\text{bdry}}$.

For an integer $s > 0$, define the *broken Sobolev space* $H^s(\mathcal{T}_h)$ by

$$H^s(\mathcal{T}_h) := \{v \in L^2(\Omega) : v|_K \in H^s(K), \forall K \in \mathcal{T}_h\},$$

and on this space define the inner product $(v_h, w_h)_{s,h} := \sum_{K \in \mathcal{T}_h} (D^s v_h, D^s w_h)_K$, with the broken H^s seminorm

$$|v_h|_{s,h}^2 := \sum_{K \in \mathcal{T}_h} |v_h|_{s,K}^2.$$

For a function $v \in H^2(\mathcal{T}_h)$ we define the jump operator $[\cdot]$ across an edge $e \in \mathcal{E}_h$ as follows. For an internal edge, $e \in \mathcal{E}_h^{\text{int}}$, define $[v] := v^+ - v^-$ where v^\pm denotes the trace of $v|_{K^\pm}$ where $e \subset \partial K^+ \cap \partial K^-$. For boundary edges, $e \in \mathcal{E}_h^{\text{bdry}}$, let $[v] := v|_e$.

Definition 2.1. We define the H^2 -nonconforming space as follows.

$$H_\ell^{2,nc}(\mathcal{T}_h) := \{v \in H^2(\mathcal{T}_h) : v \text{ is continuous at the vertices, } \int_e [v] p \, ds = 0 \, \forall p \in \mathbb{P}_{\ell-3}(e), \, \forall e \in \mathcal{E}_h^{\text{int}}, \\ \int_e [\partial_n v] p \, ds = 0 \, \forall p \in \mathbb{P}_{\ell-2}(e), \, \forall e \in \mathcal{E}_h\}.$$

We also make the following regularity conditions on the mesh \mathcal{T}_h .

Assumption 2.2 (Mesh assumptions). Assume there exists some $\rho > 0$ such that the following holds.

- For every element $K \in \mathcal{T}_h$ and every $e \subset \partial K$, $h_e \geq \rho h_K$ where $h_e = |e|$.
- Each element $K \in \mathcal{T}_h$ is star shaped with respect to a ball of radius ρh_K .

Note that Assumption 2.2 is standard in the VEM framework (see e.g. [8]).

Remark 2.3. We note that from Assumption 2.2 we can show that there exists an interior point x_K to K such that the sub triangle formed by connecting x_K to the vertices of K is made of shape regular triangles. This property considered also in [4], is necessary for the proof of Lemma 4.8.

For any $K \in \mathcal{T}_h$ we define the orthogonal $L^2(K)$ projection onto the space $\mathbb{P}_\ell(K)$, that is $\mathcal{P}_\ell^K : L^2(K) \rightarrow \mathbb{P}_\ell(K)$, as the solution of

$$(\mathcal{P}_\ell^K v, p)_K = (v, p)_K \quad \forall p \in \mathbb{P}_\ell(K).$$

We also recall the following approximation results for the L^2 projection. A proof of the following can be obtained using for example the theory in [12].

Theorem 2.4. Under Assumption 2.2, for $\ell \geq 0$ and for any $w \in H^m(K)$ with $1 \leq m \leq \ell + 1$, it follows that

$$|w - \mathcal{P}_\ell^K w|_{s,K} \lesssim h_K^{m-s} |w|_{m,K}$$

for $s = 0, 1, 2$ with $s \leq m$. Further, for any edge shared by $K^+, K^- \in \mathcal{T}_h$ and for any $w \in H^m(K^+ \cup K^-)$, with $1 \leq m \leq \ell + 1$, it follows that

$$|w - \mathcal{P}_\ell^e w|_{s,e} \lesssim h_e^{m-s-\frac{1}{2}} |w|_{m,K^+ \cup K^-}$$

for $s = 0, 1, 2$ with $s \leq m$.

Finally, we use the following notation for the local bilinear form $a^K(\cdot, \cdot)$. For $K \in \mathcal{T}_h$, define a^K as follows

$$a^K(v, w) = \int_K D^2 v : D^2 w \, dx \quad \forall v, w \in V.$$

3 Virtual element discretization

In this section we construct the VEM discretization. This involves building the discrete virtual element space, $V_{h,\ell}$, the projection operators, and the discrete forms. The first step in constructing the VEM space $V_{h,\ell}$ is to introduce an enlarged space $\tilde{V}_{h,\ell}^K$ and an extended set of dofs for this space. We then introduce a suitable set of dofs for $V_{h,\ell}^K$ and use these dofs to construct the *dof compatible* projection operators $\Pi_0^K, \Pi_1^K, \Pi_2^K$ which will be used to define the local VEM space as well as the local discrete forms. The projections have the advantage of being defined based on a constraint least squares problem and are fully computable using the dofs. Note that the construction is identical to the method employed in [21] where any omitted details can be found. Throughout this section and the remainder of the paper we assume that $\ell \geq 2$.

3.1 Local VEM space

Following the standard VEM enhancement technique [1, 16] we first give the definition of the local enlarged VEM space $\tilde{V}_{h,\ell}^K$ for $K \in \mathcal{T}_h$.

Definition 3.1 (Local enlarged space). *Given an element $K \in \mathcal{T}_h$ the local enlarged space $\tilde{V}_{h,\ell}^K$ is defined as*

$$\tilde{V}_{h,\ell}^K = \{v_h \in H^2(K) : \Delta^2 v_h \in \mathbb{P}_\ell(K), v_h|_e \in \mathbb{P}_\ell(e), \Delta v_h|_e \in \mathbb{P}_{\ell-2}(e), \forall e \subset \partial K\}.$$

Definition 3.2. *For $v_h \in H^2(K)$, and given integers d_0^e and d_0^i , we define the set of dofs $\Lambda^K(d_0^e, d_0^i)$ as the following.*

(D1) *The values of v_h at each vertex v of K .*

(D2) *The moments of v_h up to order d_0^e on each $e \subset \partial K$,*

$$\frac{1}{|e|} \int_e v_h p \, ds \quad \forall p \in \mathbb{P}_{d_0^e}(e).$$

(D3) *The moments of $\partial_n v_h$ up to order $\ell - 2$ on each $e \subset \partial K$,*

$$\int_e \partial_n v_h p \, ds \quad \forall p \in \mathbb{P}_{\ell-2}(e).$$

(D4) *The moments of v_h up to order d_0^i inside K ,*

$$\frac{1}{|K|} \int_K v_h p \, dx \quad \forall p \in \mathbb{P}_{d_0^i}(K).$$

It is worth noting that depending on the basis choice for the polynomial spaces in Definition 3.2, the degrees of freedom need to be scaled appropriately. This is to ensure that the stabilization part of the discrete bilinear form satisfies standard stability properties which we discuss later in this section.

Remark 3.3. *Adopting the notation in [21], we point out that a set of dofs $\Lambda^K(d_0^e, d_0^i)$ described by Definition 3.2 corresponds to the dof tuple $(0, -1, d_0^e, \ell - 2, d_0^i)$.*

For a set of dofs described by Definition 3.2, we fix (D1) as function values at the vertices of K and we fix edge normal moments up to $\ell - 2$ in (D3). We then define the edge moments up to order d_0^e in (D2) and define inner moments up to order d_0^i in (D4). The local enlarged space (Definition 3.1) is therefore characterized by the extended set of degrees of freedom $\Lambda^K(\ell - 2, \ell)$. This set of dofs is unisolvent over the space $\tilde{V}_{h,\ell}^K$ [21]. The local VEM space $V_{h,\ell}^K \subset \tilde{V}_{h,\ell}^K$ is characterized by taking $d_0^e = \ell - 3$ and $d_0^i = \ell - 4$ in Definition 3.2, to get a set of dofs $\Lambda^K(\ell - 3, \ell - 4)$. Note that this set of dofs is identical to the set used in [4] for the biharmonic problem and they are visualized on triangles in Figure 1.

In order to define the local VEM space we now introduce the following projection operators:

- An element value projection $\Pi_0^K : \tilde{V}_{h,\ell}^K \rightarrow \mathbb{P}_\ell(K)$.
- An edge value projection $\Pi_0^e : \tilde{V}_{h,\ell}^K \rightarrow \mathbb{P}_\ell(e)$.
- An edge normal projection $\Pi_1^e : \tilde{V}_{h,\ell}^K \rightarrow \mathbb{P}_{\ell-1}(e)$.

As in [21], we consider projection operators obtained from the following constraint least squares problem.

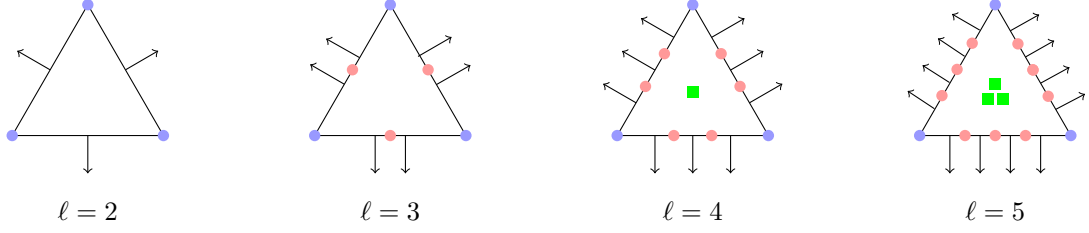


Figure 1: Degrees of freedom for polynomial orders $\ell = 2, 3, 4, 5$ on triangles for the local VEM space. Circles at vertices represent vertex dofs, arrows represent edge normal dofs, circles on edges represent edge value moments and interior squares represent inner dofs.

Definition 3.4 (Value projections). *We define the symmetric, positive definite stabilization bilinear form $S^K(\cdot, \cdot)$ as follows*

$$S^K(v_h, w_h) := \sum_{\lambda_j \in \Lambda^K(\ell-3, \ell-4)} \lambda_j(v_h) \lambda_j(w_h) \quad \forall v_h, w_h \in \tilde{V}_{h,\ell}^K. \quad (3.1)$$

We define the value projection $\Pi_0^K v_h$ as the solution to the problem

$$\begin{aligned} \text{Minimize:} \quad & S^K(\Pi_0^K v_h - v_h, \Pi_0^K v_h - v_h), \\ \text{subject to:} \quad & \int_K \Pi_0^K v_h p \, dx = \int_K v_h p \, dx \quad \forall p \in \mathbb{P}_{\ell-4}(K). \end{aligned}$$

We define the edge projection as the unique solution in $\mathbb{P}_\ell(e)$ of

$$\begin{aligned} \int_e \Pi_0^\ell v_h p \, ds &= \int_e v_h p \, ds & \forall p \in \mathbb{P}_{\ell-3}(e), \\ \int_e \Pi_0^\ell v_h p \, ds &= \int_e \Pi_0^K v_h p \, ds & \forall p \in \mathbb{P}_{\ell-2}(e) \setminus \mathbb{P}_{\ell-3}(e), \\ \Pi_0^\ell v_h(e^\pm) &= v_h(e^\pm). \end{aligned}$$

We define the edge normal projection as the unique solution in $\mathbb{P}_{\ell-1}(e)$ of

$$\begin{aligned} \int_e \Pi_1^\ell v_h p \, ds &= \int_e \partial_n v_h p \, ds & \forall p \in \mathbb{P}_{\ell-2}(e), \\ \int_e \Pi_1^\ell v_h p \, ds &= \int_e \partial_n (\Pi_0^K v_h) p \, ds & \forall p \in \mathbb{P}_{\ell-1}(e) \setminus \mathbb{P}_{\ell-2}(e). \end{aligned}$$

In order to construct a gradient projection which is exact, we use the value projection in the definition of the edge projection. Otherwise, we are only able to define the edge projection into $\mathbb{P}_{\ell-1}(e)$ and do not have sufficient moments on the edge to show that the gradient projection is exact. In turn, this means that the edge projection depends on both e and K . Similarly, we also use the value projection to construct the edge normal projection into $\mathbb{P}_{\ell-1}(e)$, but in contrast, an edge normal projection defined into $\mathbb{P}_{\ell-2}(e)$ is sufficient to define an exact hessian projection. For more details see the discussion in [21].

Finally, we are able to use the projections defined in Definition 3.4 to define both the gradient Π_1^K and hessian Π_2^K projections.

Definition 3.5 (Gradient projection). *The gradient projection $\Pi_1^K : \tilde{V}_{h,\ell}^K \rightarrow [\mathbb{P}_{\ell-1}(K)]^2$ is defined as*

$$\int_K \Pi_1^K v_h p \, dx = - \int_K \Pi_0^K v_h \nabla p \, dx + \sum_{e \subset \partial K} \int_e \Pi_0^\ell v_h p n \, ds, \quad \forall p \in [\mathbb{P}_{\ell-1}(K)]^2.$$

Definition 3.6 (Hessian projection). *The hessian projection $\Pi_2^K : \tilde{V}_{h,\ell}^K \rightarrow [\mathbb{P}_{\ell-2}(K)]^{2 \times 2}$ is defined as*

$$\int_K \Pi_2^K v_h p \, dx = - \int_K \Pi_1^K v_h \otimes \nabla p \, dx + \sum_{e \subset \partial K} \int_e (\Pi_1^\ell v_h n \otimes np + \partial_s (\Pi_0^\ell v_h) \tau \otimes np) \, ds, \quad \forall p \in [\mathbb{P}_{\ell-2}(K)]^{2 \times 2}.$$

Here n, τ denote the unit normal and tangent vectors of e , respectively.

By defining the projections in this way, it follows that they are indeed computable from the dofs [21].

Definition 3.7. *We use the notation Π_0^h, Π_1^h and Π_2^h to denote the global value, gradient, and hessian projections, respectively. Therefore for $s = 0, 1, 2$,*

$$(\Pi_s^h v_h)|_K := \Pi_s^K v_h \quad \forall v_h \in V_{h,\ell}.$$

Using Definition 3.4 we can now define the local virtual space. This is given as follows.

Definition 3.8 (Local virtual space). *The local virtual element space $V_{h,\ell}^K$ is defined as*

$$V_{h,\ell}^K := \left\{ v_h \in \tilde{V}_{h,\ell}^K : (v_h - \Pi_0^K v_h, p)_K = 0 \quad \forall p \in \mathbb{P}_\ell(K) \setminus \mathbb{P}_{\ell-4}(K), \right. \\ \left. (v_h - \Pi_0^e v_h, p)_e = 0 \quad \forall p \in \mathbb{P}_{\ell-2}(e) \setminus \mathbb{P}_{\ell-3}(e) \right\}. \quad (3.2)$$

The set of local degrees of freedom $\Lambda^K(\ell-3, \ell-4)$ is unisolvent over $V_{h,\ell}^K$. A proof of this can be found in [21]. Also shown in [21] is the proof of the subsequent lemma, detailing that all the projections satisfy a crucial L^2 projection property. This property follows as a consequence of the construction of the value, gradient, and hessian projections.

Lemma 3.9. *The value, gradient, and hessian projections satisfy*

$$\Pi_s^K v_h = \mathcal{P}_{\ell-s}^K(D^s v_h) \quad \forall v_h \in V_{h,\ell}^K, \quad s = 0, 1, 2. \quad (3.3)$$

It also holds that $\mathbb{P}_\ell(K) \subset V_{h,\ell}^K$ and therefore

$$\Pi_s^K p = D^s p \quad \forall p \in \mathbb{P}_\ell(K), \quad s = 0, 1, 2. \quad (3.4)$$

3.2 Global spaces and the discrete forms

The global VEM space can now be defined in the standard way as follows.

Definition 3.10 (Global virtual space). *The global VEM space is defined as*

$$V_{h,\ell} := \left\{ v_h \in H_\ell^{2,nc}(\mathcal{T}_h) : v_h|_K \in V_{h,\ell}^K \quad \forall K \in \mathcal{T}_h \right\} \quad (3.5)$$

where $H_\ell^{2,nc}(\mathcal{T}_h)$ is the nonconforming space given in Definition 2.1.

As usual, we can define the corresponding global dofs as an extension to those described in Definition 3.2 with $d_0^e = \ell - 3$ and $d_0^v = \ell - 4$. We can extend (D1) to evaluation at internal vertices, (D2) and (D3) to internal edges $e \in \mathcal{E}_h^{\text{int}}$, and finally we can take (D4) for each $K \in \mathcal{T}_h$. We set the local normal dofs which correspond to boundary edges to zero. Note that the global degrees of freedom are unisolvent - this follows from the unisolvency of the local degrees of freedom and the definition of the local spaces.

Now that the virtual spaces and projection operators are in place, we are able to define the discrete bilinear forms.

Definition 3.11 (Discrete forms). *For $v_h, w_h, z_h \in V_{h,\ell}$ define the discrete forms as*

$$a_h^K(v_h, w_h) = \int_K \Pi_2^K v_h : \Pi_2^K w_h \, dx + h_K^{-2} S^K(v_h - \Pi_0^K v_h, w_h - \Pi_0^K w_h), \\ m_h^K(v_h, w_h) = \int_K \Pi_0^K v_h \Pi_0^K w_h \, dx + h_K^2 S^K(v_h - \Pi_0^K v_h, w_h - \Pi_0^K w_h), \\ r_h^K(z_h; v_h, w_h) = \int_K \phi'(z_h) \Pi_1^K v_h \cdot \Pi_1^K w_h \, dx + \beta_K S^K(v_h - \Pi_0^K v_h, w_h - \Pi_0^K w_h),$$

where $S^K(\cdot, \cdot)$ has been defined previously in (3.1), and β_K is constant.

Remark 3.12. *Note that the value projection will be used in the first argument of $r_h^K(\cdot; \cdot, \cdot)$ in order to define the semidiscrete scheme which we delay until Section 4.1. However, we need the form as it is to be able to apply it to u which is necessary for the analysis.*

Due to Lemma 3.9 it is immediate that the discrete forms $a_h^K(\cdot, \cdot)$ and $m_h^K(\cdot, \cdot)$ possess the standard consistency property, implying that whenever one of the entries in the bilinear form is a polynomial of degree ℓ , the form is exact.

Lemma 3.13 (Polynomial consistency). *For any $w_h \in V_{h,\ell}$, it holds that*

$$a_h^K(p, w_h) = a^K(p, w_h), \quad m_h^K(p, w_h) = (p, w_h)_K$$

for all $p \in \mathbb{P}_\ell(K)$.

We also have the standard stability property for these forms. The proof is standard and is based on a scaling argument: in the conforming case it can be found for example in [9, 13] and the nonconforming case is shown in [41] but for a different choice of stabilization $S^K(\cdot, \cdot)$.

Lemma 3.14 (Stability). *There exists positive constants $\alpha_*, \alpha^*, \mu_*$, and μ^* such that for all $v_h \in V_{h,\ell}^K$*

$$\begin{aligned}\alpha_* a^K(v_h, v_h) &\leq a_h^K(v_h, v_h) \leq \alpha^* a^K(v_h, v_h), \\ \mu_* (v_h, v_h)_K &\leq m_h^K(v_h, v_h) \leq \mu^* (v_h, v_h)_K.\end{aligned}$$

The global forms can be defined in the usual way, for $z_h, v_h, w_h \in V_{h,\ell}$,

$$\begin{aligned}a_h(v_h, w_h) &:= \sum_{K \in \mathcal{T}_h} a_h^K(v_h, w_h), \quad m_h(v_h, w_h) := \sum_{K \in \mathcal{T}_h} m_h^K(v_h, w_h), \\ r_h(z_h; v_h, w_h) &:= \sum_{K \in \mathcal{T}_h} r_h^K(z_h; v_h, w_h).\end{aligned}$$

Finally, we assume that there exists the interpolation operator I_h , defined in the usual way, which satisfies interpolation estimates [8, 42] i.e. under Assumption 2.2 for $s = 0, 1, 2$ and any $w \in H^m(K)$ with $s \leq m \leq \ell + 1$ the following estimate holds

$$|w - I_h w|_{s,K} \lesssim h^{m-s} |w|_{m,K}. \quad (3.6)$$

4 Error analysis of the semidiscrete scheme

In this section we detail the error analysis for the semidiscrete (continuous-in-time) scheme. Focusing on the spatial discretization, we present the semidiscrete scheme in (4.1) and prove L^2 convergence in Theorem 4.9. Standard arguments can be employed in the fully discrete case (using the methods for example in [44]).

4.1 The semidiscrete problem

The semidiscrete problem is defined as follows: find $u_h(\cdot, t) \in V_{h,\ell}$ such that

$$\begin{aligned}m_h(\partial_t u_h, v_h) + \varepsilon^2 a_h(u_h, v_h) + r_h(\Pi_0^h u_h; u_h, v_h) &= 0 \quad \forall v_h \in V_{h,\ell}, \text{ a.e. } t \text{ in } (0, T), \\ u_h(\cdot, 0) &= u_{h,0}(\cdot) \in V_{h,\ell},\end{aligned} \quad (4.1)$$

where $u_{h,0}$ is some approximation of u_0 and the discrete forms are given in Definition 3.11.

We make the following assumption on the discrete solution u_h of (4.1), which is standard and well accepted in the analysis of this problem [3]. For more details on this assumption and for a full justification see [29].

Assumption 4.1. *The solution u_h to (4.1) satisfies for all $t \in (0, T]$*

$$\|u_h(\cdot, t)\|_{1,\infty;h} \leq C_T$$

for a constant C_T independent of h , which depends on T , where

$$\|v_h\|_{m,\infty;h} := \max_{\substack{1 \leq j \leq m \\ K \in \mathcal{T}_h}} |v_h|_{j,\infty,K}.$$

Note that in the following we do not include the dependence of u and u_h on time t and the bounds involving u or u_h hold for all $t \in (0, T]$. The proof techniques in this chapter follow along the lines of [3].

4.2 The elliptic projection

In this subsection we introduce the elliptic projection, which is fundamental for the proof of the main L^2 convergence theorem detailed in Theorem 4.9. To this end, we define the elliptic projection $P_h v \in V_{h,\ell}$ for $v \in H^4(\Omega)$ as the solution of

$$b_h(P_h v, \psi_h) = (\varepsilon^2 \Delta^2 v - \nabla \cdot (\phi'(u) \nabla v) + \alpha v, \psi_h) \quad \forall \psi_h \in V_{h,\ell} \quad (4.2)$$

where the bilinear form $b_h(\cdot, \cdot)$ is defined as

$$b_h(v_h, w_h) := \varepsilon^2 a_h(v_h, w_h) + r_h(u; v_h, w_h) + \alpha(v_h, w_h), \quad (4.3)$$

for a positive α , chosen so that the bilinear form b_h is coercive.

The main results of this section are the approximation properties of P_h detailed in Lemma 4.3. Before we state these properties, we require the following lemma, the proof of which can be found in [21].

Lemma 4.2. For the solution $u \in H^{\ell+1}(\Omega)$ to (2.1) and $w \in H_\ell^{2,nc}(\mathcal{T}_h)$ the nonconformity error satisfies

$$|\mathcal{N}(u, w)| = \left| \varepsilon^2 \sum_{K \in \mathcal{T}_h} \int_{\partial K} ((\Delta u - \partial_{ss} u) \partial_n w + \partial_{ns} u \partial_s w - \partial_n (\Delta u) w) \, ds \right| \lesssim h^{\ell-1} |w|_{2,h},$$

where the nonconformity error is defined as follows

$$\mathcal{N}(u, w) := \varepsilon^2 \sum_{K \in \mathcal{T}_h} a^K(u, w) - (\Delta^2 u, w). \quad (4.4)$$

Lemma 4.3. Let $u \in H^4(\Omega) \cap H^{\ell+1}(\Omega)$ be the solution to (2.1) and let $P_h u$ be the elliptic projection defined in (4.2). Then, it holds that

$$\|u - P_h u\|_{2,h} \lesssim h^{\ell-1}, \quad (4.5)$$

$$\|u - P_h u\|_{1,h} \lesssim h^\ell, \quad (4.6)$$

$$\|u_t - (P_h u)_t\|_{2,h} \lesssim h^{\ell-1}, \quad (4.7)$$

$$\|u_t - (P_h u)_t\|_{1,h} \lesssim h^\ell. \quad (4.8)$$

Proof of the estimate (4.5) in Lemma 4.3 is a direct consequence of the energy norm convergence proof covered in [21, Theorem 5.7] for a general fourth-order problem with varying coefficients.

In order to prove (4.6) we first study the following problem: find $z \in V$ such that

$$b(z, w) = (u - P_h u, w)_{1,h} + (u - P_h u, w)_{0,h} =: L_h(w) \quad \forall w \in V \quad (4.9)$$

where the bilinear form $b(\cdot, \cdot)$ is defined as

$$b(v, w) := \varepsilon^2 a(v, w) + r(u; v, w) + \alpha(v, w)$$

for all $v, w \in V$. We assume the validity of the following regularity result which is shown in the case of a rectangular domain in [29]: there exists a solution $z \in H^3(\Omega)$ to (4.9) such that

$$\|z\|_{3,\Omega} \leq C_\Omega \|u - P_h u\|_{1,h}, \quad (4.10)$$

where C_Ω depends only on Ω .

Lemma 4.4. Let $u \in H^4(\Omega) \cap H^{\ell+1}(\Omega)$ be the solution to (2.1) and let $P_h u$ be the elliptic projection defined in (4.2). For the solution $z \in H^3(\Omega)$ of the dual problem (4.9), it holds that

$$|b(z, u - P_h u)| \lesssim h^\ell \|u - P_h u\|_{1,h}. \quad (4.11)$$

We give the proof of Lemma 4.4 in Appendix A. Also necessary for the proof of (4.7)-(4.8) in Lemma 4.3 is the following lemma, the proof is given in Appendix A.

Lemma 4.5. Let $u \in H^4(\Omega) \cap H^{\ell+1}(\Omega)$ be the solution to (2.1) and let $P_h u$ be the elliptic projection defined in (4.2). For any $\eta_h \in V_{h,\ell}$, it holds

$$|(\phi''(u) u_t \Pi_1^K P_h u, \Pi_1^K \eta_h)_{0,h} - (\phi''(u) u_t \nabla u, \nabla \eta_h)_{0,h}| \lesssim h^\ell \|\eta_h\|_{2,h}.$$

We now give the proof of Lemma 4.3.

Proof of Lemma 4.3. Define $\rho := u - P_h u$. Then, it follows that

$$\|\rho\|_{1,h}^2 = [L_h(\rho) - b(z, \rho)] + b(z, \rho) = I + II.$$

In view of Lemma 4.4 we need only estimate term I . To this end, we use the same technique considered in [48] for proving H^1 estimates for the fourth-order plate bending problem and introduce the interpolation v_h^* into the lowest order H^1 -conforming VEM space presented in e.g. [8]. The following estimate therefore holds. For any $w \in H^2(K)$, there exists w^* in the lowest order H^1 -conforming VEM space such that

$$\|w - w^*\|_{0,K} + h_K |w - w^*|_{1,K} \lesssim h_K^2 |w|_{2,K}. \quad (4.12)$$

Notice that it also follows from [29, (5.6)] using the density of V in H^1 that for any $v \in H^1(\Omega)$

$$\varepsilon^2 (-\nabla \Delta z, \nabla v) + r(u; z, v) + \alpha(z, v) = L_h(v). \quad (4.13)$$

Therefore, using (4.13) with $v = \rho^*$ we see that

$$I = L_h(\rho) - b(z, \rho) + \varepsilon^2 (-\nabla \Delta z, \nabla \rho^*) + r(u; z, \rho^*) + \alpha(z, \rho^*) - L_h(\rho^*)$$

$$= L_h(\rho - \rho^*) - \varepsilon^2(D^2 z, D^2 \rho) + \varepsilon^2(-\nabla \Delta z, \nabla \rho^*) + r(u; z, \rho^* - \rho) + \alpha(z, \rho^* - \rho).$$

We also observe that the following holds using integration by parts

$$\varepsilon^2(D^2 z, D^2 \rho) = -\varepsilon^2(\nabla \Delta z, \nabla \rho) + \varepsilon^2 \sum_{K \in \mathcal{T}_h} \int_{\partial K} ((\Delta z - \partial_{ss} z) \partial_n \rho + \partial_{ns} z \partial_s \rho) \, ds$$

and so, after combining this with the expression for I , we get

$$\begin{aligned} I &= L_h(\rho - \rho^*) + \varepsilon^2(\nabla \Delta z, \nabla(\rho - \rho^*)) + r(u; z, \rho^* - \rho) + \alpha(z, \rho^* - \rho) \\ &\quad + \varepsilon^2 \sum_{K \in \mathcal{T}_h} \int_{\partial K} ((\Delta z - \partial_{ss} z) \partial_n \rho + \partial_{ns} z \partial_s \rho) \, ds =: I_1 + I_2 + I_3 + I_4 + I_5. \end{aligned}$$

Using Cauchy-Schwarz and (3.6) it holds that

$$\begin{aligned} I_1 &\leq |L_h(\rho - \rho^*)| = \left| \sum_{K \in \mathcal{T}_h} \int_K \nabla \rho \cdot \nabla(\rho - \rho^*) + \rho(\rho - \rho^*) \, dx \right| \leq \sum_{K \in \mathcal{T}_h} \|\rho\|_{1,K} \|\rho - \rho^*\|_{1,K} \\ &\lesssim \|u - P_h u\|_{1,h} h \|u - P_h u\|_{2,h} \lesssim h^\ell \|u - P_h u\|_{1,h}. \end{aligned}$$

In the last step we have applied (4.5). Similarly for the next three terms, we can apply the lowest order conforming interpolation estimates from (4.12), the properties of the elliptic projection (4.5) and the regularity results (4.10), yielding

$$\begin{aligned} I_2 &\leq |\varepsilon^2(\nabla \Delta z, \nabla(\rho - \rho^*))| \lesssim \varepsilon^2 \|z\|_{3,\Omega} h \|u - P_h u\|_{2,h} \lesssim h^\ell \|u - P_h u\|_{1,h}, \\ I_3 &\leq |r(u; z, \rho^* - \rho)| \lesssim h \|z\|_{3,\Omega} \|u - P_h u\|_{2,h} \lesssim h^\ell \|u - P_h u\|_{1,h}, \\ I_4 &\leq |\alpha(z, \rho^* - \rho)| \lesssim h \|z\|_{3,\Omega} \|u - P_h u\|_{2,h} \lesssim h^\ell \|u - P_h u\|_{1,h}. \end{aligned}$$

Finally, we notice that I_5 can be estimated using the same method as in Lemma 4.2, the proof of which can be found in [21, Theorem 5.5]. Therefore

$$I \lesssim h^\ell \|u - P_h u\|_{1,h}$$

and (4.6) holds.

It remains to show (4.7)-(4.8). For this, we notice that for any $w_h \in V_{h,\ell}$

$$b_h((P_h u)_t, w_h) = b(u_t, w_h) - \mathcal{N}(u_t, w_h) + (\phi''(u) u_t \nabla u, \nabla w_h) - (\phi''(u) u_t \Pi_1^K P_h u, \Pi_1^K w_h). \quad (4.14)$$

Using the coercivity of the bilinear form b_h , alongside (4.14) and the definition of $P_h u$, we have the following

$$\begin{aligned} \|P_h(u_t) - (P_h u)_t\|_{2,h}^2 &\lesssim b_h(P_h(u_t) - (P_h u)_t, P_h(u_t) - (P_h u)_t) \\ &= b_h(P_h(u_t), P_h(u_t) - (P_h u)_t) - b_h((P_h u)_t, P_h(u_t) - (P_h u)_t) \\ &= (\phi''(u) u_t \Pi_1^K P_h u, \Pi_1^K (P_h(u_t) - (P_h u)_t)) - (\phi''(u) u_t \nabla u, \nabla (P_h(u_t) - (P_h u)_t)) \\ &\lesssim h^\ell \|P_h(u_t) - (P_h u)_t\|_{2,h}, \end{aligned}$$

where we have applied Lemma 4.5 with $\eta_h = P_h(u_t) - (P_h u)_t$ in the last step. It therefore follows that

$$\|u_t - (P_h u)_t\|_{2,h} \leq \|u_t - P_h(u_t)\|_{2,h} + \|P_h(u_t) - (P_h u)_t\|_{2,h} \lesssim h^{\ell-1}.$$

In order to prove (4.8), we proceed in the exact same way as the proof of (4.6). We consider again a dual problem: find $\tilde{z} \in V$ such that

$$b(\tilde{z}, w) = (u_t - (P_h u)_t, w)_{1,h} + (u_t - (P_h u)_t, w)_{0,h} \quad \forall w \in V.$$

We can then use Lemma 4.5 with $\eta_h = I_h \tilde{z}$ as well as a regularity result for \tilde{z} to show that

$$|b(\tilde{z}, u_t - (P_h u)_t)| \lesssim h^\ell \|u_t - (P_h u)_t\|_{1,h}$$

and the result follows as before. \square

Remark 4.6. Notice that it follows from (3.6) and (4.6) as well as stability properties of the interpolation operator that the elliptic projection is bounded [29]. In particular,

$$\|P_h u\|_{1,\infty;h} \leq C. \quad (4.15)$$

We use this property in the proof of some technical lemmas described in the next subsection.

4.3 Technical results

This intermediate subsection is dedicated to two additional preliminary results that are required before we can prove the L^2 error estimate presented in Theorem 4.9. The first is an estimate for the semilinear term r_h . We use the following standard error decomposition arising in the study of time-dependent problems:

$$u - u_h = (u - P_h u) + (P_h u - u_h) =: \rho + \theta, \quad (4.16)$$

for u the solution to (2.1) and $P_h u$ the projection defined in (4.2).

Lemma 4.7. *If $u \in H^4(\Omega) \cap H^{\ell+1}(\Omega)$ it follows that*

$$|r_h(\Pi_0^h u_h; u_h, \theta) - r_h(u; P_h u, \theta)| \lesssim (|\theta|_{1,h} + \|\theta\|_{0,h} + \|\rho\|_{0,h} + h^\ell) |\theta|_{1,h}. \quad (4.17)$$

Proof. Using the definition of r_h we have that

$$\begin{aligned} |r_h(\Pi_0^h u_h; u_h, \theta) - r_h(u; P_h u, \theta)| &= \left| \sum_{K \in \mathcal{T}_h} \int_K (\phi'(\Pi_0^K u_h) \Pi_1^K u_h - \phi'(u) \Pi_1^K (P_h u)) \cdot \Pi_1^K \theta \, dx \right| \\ &\leq \sum_{K \in \mathcal{T}_h} \left\| \phi'(\Pi_0^K u_h) \Pi_1^K u_h - \phi'(u) \Pi_1^K (P_h u) \right\|_{0,K} |\theta|_{1,K} \end{aligned}$$

where we have used Lemma 3.9 since $\theta \in V_{h,\ell}$. Therefore, using the triangle inequality, we see that

$$\begin{aligned} \left\| \phi'(\Pi_0^K u_h) \Pi_1^K u_h - \phi'(u) \Pi_1^K (P_h u) \right\|_{0,K} &\leq \left\| \phi'(\Pi_0^K u_h) (\Pi_1^K u_h - \Pi_1^K (P_h u)) \right\|_{0,K} \\ &\quad + \left\| (\phi'(\Pi_0^K u_h) - \phi'(u)) \Pi_1^K (P_h u) \right\|_{0,K} =: J_1 + J_2. \end{aligned}$$

To estimate the first term J_1 it follows that

$$J_1 = \left\| \phi'(\Pi_0^K u_h) (\Pi_1^K u_h - \Pi_1^K (P_h u)) \right\|_{0,K} = \left\| \phi'(\Pi_0^K u_h) \Pi_1^K \theta \right\|_{0,\Omega} \lesssim |\theta|_{1,K}$$

where we have used Assumption 4.1, alongside L^∞ stability properties of the L^2 projection (for more details see e.g. the theory in [19]).

To estimate the second term J_2 , we have that

$$J_2 = \left\| (\phi'(\Pi_0^K u_h) - \phi'(u)) \Pi_1^K (P_h u) \right\|_{0,K} \lesssim \|P_h u\|_{1,\infty;h} \|\Pi_0^K u_h - u\|_{0,K}$$

where we have used the bounded property of $P_h u$ in (4.15).

Notice that using the triangle inequality, the definitions of ρ, θ , and properties of the L^2 projection, we have

$$\begin{aligned} \|\Pi_0^K u_h - u\|_{0,K} &\leq \|\Pi_0^K u_h - \Pi_0^K P_h u\|_{0,K} + \|\mathcal{P}_\ell^K P_h u - \mathcal{P}_\ell^K u\|_{0,K} + \|\mathcal{P}_\ell^K u - u\|_{0,K} \\ &= \|\Pi_0^K \theta\|_{0,K} + \|\mathcal{P}_\ell^K \rho\|_{0,K} + \|(I - \mathcal{P}_\ell^K)u\|_{0,K} \lesssim \|\theta\|_{0,K} + \|\rho\|_{0,K} + h^\ell. \end{aligned}$$

Hence, by combining the estimates for J_1 and J_2 :

$$|r_h(\Pi_0^h u_h; u_h, \theta) - r_h(u; P_h u, \theta)| \lesssim (|\theta|_{1,h} + \|\theta\|_{0,h} + \|\rho\|_{0,h} + h^\ell) |\theta|_{1,h},$$

as required. \square

We require one additional lemma. The proof is given in Appendix A.

Lemma 4.8. *For any $w_h, z_h \in V_{h,\ell}$, it holds that*

$$\left| \sum_{K \in \mathcal{T}_h} \int_{\partial K} (\partial_n z_h) w_h \, ds \right| \lesssim h (|w_h|_{1,h} |z_h|_{2,h} + |w_h|_{2,h} |z_h|_{2,h}). \quad (4.18)$$

4.4 Error estimate for the semidiscrete scheme

In this subsection we prove the error estimate for the scheme detailed in (4.1).

Theorem 4.9. *Assume that $u \in H^4(\Omega) \cap H^{\ell+1}(\Omega)$ is the solution to the continuous problem (2.1) and u_h is the solution to (4.1). Then, for all $t \in [0, T]$,*

$$\|u - u_h\|_{0,h} \lesssim h^\ell. \quad (4.19)$$

Proof. Recall the error decomposition detailed in (4.16), and notice that due to Lemma 4.3, we need only estimate θ . Following the ideas in [3], we use the definition of θ and the semidiscrete scheme (4.1) to show that

$$\begin{aligned} m_h(\theta_t, \chi_h) + \varepsilon^2 a_h(\theta, \chi_h) &= m_h((P_h u)_t, \chi_h) + \varepsilon^2 a_h(P_h u, \chi_h) - (m_h((u_h)_t, \chi_h) + \varepsilon^2 a_h(u_h, \chi_h)) \\ &= m_h((P_h u)_t, \chi_h) + \varepsilon^2 a_h(P_h u, \chi_h) + r_h(\Pi_0^h u_h; u_h, \chi_h). \end{aligned} \quad (4.20)$$

Using the definition of the elliptic projection in (4.2) and (4.3), it follows that

$$\begin{aligned} \varepsilon^2 a_h(P_h u, \chi_h) &= b_h(P_h u, \chi_h) - r_h(u; P_h u, \chi_h) - \alpha(P_h u, \chi_h) \\ &= (\varepsilon^2 \Delta^2 u - \nabla \cdot (\phi'(u) \nabla u) + \alpha u, \chi_h) - r_h(u; P_h u, \chi_h) - \alpha(P_h u, \chi_h). \end{aligned}$$

Therefore, substituting this into (4.20) we see that

$$\begin{aligned} m_h(\theta_t, \chi_h) + \varepsilon^2 a_h(\theta, \chi_h) &= m_h((P_h u)_t, \chi_h) + (\varepsilon^2 \Delta^2 u - \nabla \cdot (\phi'(u) \nabla u), \chi_h) \\ &\quad + \alpha(u - P_h u, \chi_h) + r_h(\Pi_0^h u_h; u_h, \chi_h) - r_h(u; P_h u, \chi_h) \\ &= m_h((P_h u)_t, \chi_h) - (u_t, \chi_h) + \alpha(\rho, \chi_h) + r_h(\Pi_0^h u_h; u_h, \chi_h) - r_h(u; P_h u, \chi_h). \end{aligned} \quad (4.21)$$

Following the same method used in [49], combined with polynomial consistency from Lemma 3.13, it follows that

$$\begin{aligned} |m_h((P_h u)_t, \chi_h) - (u_t, \chi_h)| &= \left| \sum_{K \in \mathcal{T}_h} m_h^K((P_h u)_t, \chi_h) - (u_t, \chi_h)_K \right| \\ &= \left| \sum_{K \in \mathcal{T}_h} m_h^K((P_h u)_t - \mathcal{P}_\ell^K u_t, \chi_h) - (u_t - \mathcal{P}_\ell^K u_t, \chi_h)_K \right| \\ &\lesssim \sum_{K \in \mathcal{T}_h} \|(P_h u)_t - \mathcal{P}_\ell^K u_t\|_{0,K} \|\chi_h\|_{0,K} + \|u_t - \mathcal{P}_\ell^K u_t\|_{0,K} \|\chi_h\|_{0,K}. \end{aligned}$$

Where we have used stability of the bilinear form (Lemma 3.14) in the last step. We now use Lemma 4.3 and properties of the L^2 projection detailed in Theorem 2.4, to show that

$$|m_h((P_h u)_t, \chi_h) - (u_t, \chi_h)| \lesssim h^\ell \|\chi_h\|_{0,h}.$$

Now, we take $\chi_h = \theta$ in (4.21) and see that

$$m_h(\theta_t, \theta) + \varepsilon^2 a_h(\theta, \theta) = m_h((P_h u)_t, \theta) - (u_t, \theta) + \alpha(\rho, \theta) + r_h(\Pi_0^h u_h; u_h, \theta) - r_h(u; P_h u, \theta).$$

Using stability properties of the discrete forms alongside Lemmas 4.3 and 4.7, it holds that

$$\begin{aligned} \frac{1}{2} \frac{d}{dt} \|\theta\|_{0,h}^2 + \varepsilon^2 |\theta|_{2,h}^2 &\lesssim (h^\ell + \alpha \|\rho\|_{0,h}) \|\theta\|_{0,h} + |r_h(\Pi_0^h u_h; u_h, \theta) - r_h(u; P_h u, \theta)| \\ &\lesssim h^\ell \|\theta\|_{0,h} + (\|\theta\|_{0,h} + h^\ell) |\theta|_{1,h}. \end{aligned}$$

After an application of Young's inequality, we get

$$\frac{1}{2} \frac{d}{dt} \|\theta\|_{0,h}^2 + \varepsilon^2 |\theta|_{2,h}^2 \lesssim h^{2\ell} + \|\theta\|_{0,h}^2 + |\theta|_{1,h}^2.$$

In order to conclude the proof, we observe that for any $v_h \in V_{h,\ell}$ and $0 < \gamma \leq \frac{1}{2}$, we can use an application of integration by parts, Cauchy-Schwarz, and Lemma 4.8, to show the following holds

$$|v_h|_{1,K}^2 = - \int_K \Delta v_h v_h \, dx + \int_{\partial K} v_h \partial_n v_h \, ds \lesssim \gamma \|\Delta v_h\|_{0,K}^2 + C_\gamma \|v_h\|_{0,K}^2 + h |v_h|_{2,K}^2.$$

Therefore $|\theta|_{1,h}^2 \lesssim (\gamma + h) |\theta|_{2,h}^2 + C_\gamma \|\theta\|_{0,h}^2$, hence assuming that γ, h are sufficiently small, it holds that

$$\frac{d}{dt} \|\theta\|_{0,h}^2 + \varepsilon^2 |\theta|_{2,h}^2 \lesssim h^{2\ell} + \|\theta\|_{0,h}^2.$$

Therefore equation (4.19) follows from an application of Gronwall's lemma. \square

5 Numerical Results

In this section we present a fully discrete scheme and investigate its behaviour numerically. The fully discrete scheme couples the VEM spatial discretization with a Runge-Kutta (RK) scheme, which combines a convex splitting (CS) method with a multi-stage additive RK method. Since we present a higher order spatial discretization we couple the VEM discretization with a higher order time stepping method. We use a nonlinear convex splitting of the energy $E(u)$, defined in (2.2), see e.g. [32, 33, 38, 43], where we split the energy into a contractive and expansive part as follows

$$E(u) = E_c(u) - E_e(u) = \int_{\Omega} \left(\frac{u^4}{4} + \frac{1}{4} + \frac{\varepsilon^2}{2} |\nabla u|^2 \right) dx - \int_{\Omega} \frac{u^2}{2} dx,$$

where $E_c(u)$ is treated implicitly while $E_e(u)$ is treated explicitly. It is straightforward to show that $E_c(u)$ and $E_e(u)$ are both convex.

Definition 5.1 (Fully discrete scheme). *We split the interval $[0, T]$ into uniform subintervals each of length $\tau = T/\hat{N}$ and discretise the solution at time t_n , $n = 0, \dots, \hat{N}$, as $u_{h\tau}^n = u_h(\cdot, t_n) \in V_{h,\ell}$. We first split the semilinear form r_h according to the convex splitting above, recalling that $\phi'(w) = 3w^2 - 1$, this is given by*

$$r_{h,c}(u_{h\tau}^n; v_h, w_h) - r_{h,e}(u_{h\tau}^n; v_h, w_h) = \sum_{K \in \mathcal{T}_h} \int_K 3(u_{h\tau}^n)^2 \Pi_1^K v_h \cdot \Pi_1^K w_h dx - \sum_{K \in \mathcal{T}_h} \int_K \Pi_1^K v_h \cdot \Pi_1^K w_h dx$$

for $u_{h\tau}^n, v_h, w_h \in V_{h,\ell}$. Our fully discrete scheme is therefore as follows: given $u_{h\tau}^0 = u_{h,0} \in V_{h,\ell}$, for $n = 0, \dots, \hat{N} - 1$, find $u_{h\tau}^{n+1} \in V_{h,\ell}$ such that

$$m_h(u_{h\tau}^{n+1} - u_{h\tau}^n, v_h) + \tau \sum_{i=1}^s \left(b_i \left(\varepsilon^2 a_h(U^i, v_h) + r_{h,c}(\Pi_0^h U^i; U^i, v_h) \right) - \hat{b}_i r_{h,e}(\Pi_0^h U^i; U^i, v_h) \right) = 0$$

where the i -th stage is defined by

$$m_h(U^i - u_{h\tau}^n, v_h) + \tau \sum_{j=1}^s \left(a_{ij} \left(\varepsilon^2 a_h(U^j, v_h) + r_{h,c}(\Pi_0^h U^j; U^j, v_h) \right) - \hat{a}_{ij} r_{h,e}(\Pi_0^h U^j; U^j, v_h) \right) = 0$$

for all $v_h \in V_{h,\ell}$, for $i = 1, \dots, s$. The coefficients are defined using standard Butcher notation for RK methods and satisfy $A, \hat{A} \in \mathbb{R}^{s \times s}$, $b, \hat{b} \in \mathbb{R}^s$.

The first scheme we use is the simple first order CS “Forward-Backward Euler” method (CSRK-1) [43], with the standard Butcher notation

$$\begin{array}{c|c} c & A \\ \hline & b^T \end{array} = \begin{array}{c|cc} 0 & 0 & 0 \\ 1 & 0 & 1 \\ \hline & 0 & 1 \end{array}, \quad \begin{array}{c|c} \hat{c} & \hat{A} \\ \hline & \hat{b}^T \end{array} = \begin{array}{c|cc} 0 & 0 & 0 \\ 1 & 1 & 0 \\ \hline & 1 & 0 \end{array}. \quad (5.1)$$

The other method we consider is the second order CS Runge-Kutta method (CSRK-2) presented in [38], rewritten in Butcher notation as

$$\begin{array}{c|c} c & A \\ \hline & b^T \end{array} = \begin{array}{c|cccc} 0 & 0 & 0 & 0 & 0 \\ 1 & 0 & 1 & 0 & 0 \\ \frac{3}{2} & 0 & \frac{1}{2} & 1 & 0 \\ 1 & 0 & 1 & -1 & 1 \\ \hline & 0 & 1 & -1 & 1 \end{array}, \quad \begin{array}{c|c} \hat{c} & \hat{A} \\ \hline & \hat{b}^T \end{array} = \begin{array}{c|cccc} 0 & 0 & 0 & 0 & 0 \\ 1 & 1 & 0 & 0 & 0 \\ \frac{3}{2} & \frac{1}{2} & 1 & 0 & 0 \\ 1 & 1 & -1 & 1 & 0 \\ \hline & 1 & -1 & 1 & 0 \end{array}. \quad (5.2)$$

The schemes defined in both (5.1) and (5.2) are shown to be energy stable for the semidiscrete (continuous-in-space) schemes [38, 43]. We *numerically* investigate the energy decay property of our proposed fully discrete scheme in Test 3 in Section 5.3.

We point out that the lowest order ($\ell = 2$) nonconforming VEM on triangles is identical to the Morley nonconforming finite element and so, with the exception of Test 1 in Section 5.1, we only investigate the behaviour of the higher order $\ell = 4$ VEM since the other case has been studied extensively in the literature.

The code we use to carry out the simulations is based on the Distributed and Unified Numerics Environment (DUNE) software framework [7] and has been implemented within the DUNE-FEM module [23]. DUNE is open source software implemented in C++, but since a user has access to a Python frontend [24], they can easily perform numerical experiments by describing mathematical models using the domain specific form language UFL [2]. Tutorials including some VEM examples can be found in [22] while further implementation details can be found in [20].

5.1 Test 1: Convergence to an exact solution

The first numerical experiment we consider is a non-physical test to recover the order of convergence presented in Theorem 4.9 as we investigate convergence to a known exact solution. In this test we reduce τ alongside h , starting with $\tau = 10^{-2}$. We fix $\varepsilon = 1/10$ for these experiments and run them on both the structured simplex “criss” grid consisting of half square triangles and a sequence of Voronoi grids discretizing the unit square $\Omega = (0, 1)^2$. The Voronoi grids are randomly seeded and smoothed using Lloyd’s algorithm. The L^2 , H^1 , and H^2 errors are computed at every time step and we present the maximum errors in each case. We set the forcing f so that the exact solution is given by

$$u(x, y, t) = \sin(2\pi t) \cos(2\pi x) \cos(2\pi y).$$

This is a modification of the test considered in e.g. [3, 17] where we have changed the exact solution to be nonlinear in t .

We investigate the convergence for polynomial orders $\ell = 2, 4$ for the CSRK-1 (5.1) and CSRK-2 (5.2) time stepping methods. For the sake of brevity we don’t show results for $\ell = 3$ but note that they are in line with expectations. The results on the simplex and Voronoi polygonal grids are shown in Tables 1-3 and Tables 4-6, respectively.

The results from this convergence test are in line with expectations. Since the CSRK-1 method is first order accurate in time and the CSRK-2 method is second order accurate, when combining one of these methods with the order ℓ VEM method, we should expect to see L^2 convergence rates of order $\min\{\ell, m\}$ where $m \in \{1, 2\}$ is the order from the CSRK- m method. To see the optimal L^2 convergence $O(h^\ell)$ (Theorem 4.9), we look at the $\ell = 2$ VEM method coupled with the CSRK-2 time stepping. These results are shown in Tables 2 and 5.

Note that the convergence rates in the H^1 and H^2 norms are also what we would expect to see if we extended Theorem 4.9 to include convergence results in both H^1 and H^2 norms according to classic FE theory. For example, the rate for the H^2 error with $\ell = 2$ is equal to 1 while the higher order is clearly visible in the $\ell = 4$, CSRK-2 results (Tables 3 and 6).

Table 1: Test 1: L^2 , H^1 , and H^2 errors and convergence rates for the convergence test with CSRK-1 time stepping and polynomial order $\ell = 2$ on a structured simplex grid.

size	dofs	h	L^2 -error	L^2 -eoc	H^1 -error	H^1 -eoc	H^2 -error	H^2 -eoc
50	121	0.2828	1.9412e-01	—	1.8409e+00	—	1.8815e+01	—
200	441	0.1414	9.1284e-02	1.09	8.5348e-01	1.11	8.9738e+00	1.07
800	1681	0.0707	4.5175e-02	1.01	4.1419e-01	1.04	4.3675e+00	1.04
3200	6561	0.0354	2.2522e-02	1.0	2.0391e-01	1.02	2.1492e+00	1.02

Table 2: Test 1: L^2 , H^1 , and H^2 errors and convergence rates for the convergence test with CSRK-2 time stepping and polynomial order $\ell = 2$. on a structured simplex grid.

size	dofs	h	L^2 -error	L^2 -eoc	H^1 -error	H^1 -eoc	H^2 -error	H^2 -eoc
50	121	0.2828	1.1203e-01	—	1.1001e+00	—	1.6705e+01	—
200	441	0.1414	2.9845e-02	1.91	3.0147e-01	1.87	8.0622e+00	1.05
800	1681	0.0707	7.3555e-03	2.02	7.6541e-02	1.98	3.9588e+00	1.03
3200	6561	0.0354	1.7710e-03	2.05	1.8949e-02	2.01	1.9692e+00	1.01

Table 3: Test 1: L^2 , H^1 , and H^2 errors and convergence rates for the convergence test with CSRK-2 time stepping and polynomial order $\ell = 4$ on a structured simplex grid.

size	dofs	h	L^2 -error	L^2 -eoc	H^1 -error	H^1 -eoc	H^2 -error	H^2 -eoc
50	511	0.2828	2.2046e-02	—	1.9803e-01	—	1.8769e+00	—
200	1921	0.1414	5.5596e-03	1.99	5.0125e-02	1.98	4.8603e-01	1.95
800	7441	0.0707	1.0552e-03	2.4	9.7040e-03	2.37	1.0401e-01	2.22
3200	29281	0.0354	1.6197e-04	2.7	1.6259e-03	2.58	2.6636e-02	1.97

Table 4: Test 1: L^2 , H^1 , and H^2 errors and convergence rates for the convergence test with CSRK-1 time stepping and polynomial order $\ell = 2$ on a Voronoi polygonal grid.

size	dofs	h	L^2 -error	L^2 -eoc	H^1 -error	H^1 -eoc	H^2 -error	H^2 -eoc
25	128	0.3288	2.5850e-01	—	2.3431e+00	—	2.2020e+01	—
100	503	0.1535	1.1302e-01	1.09	1.0281e+00	1.08	1.0548e+01	0.97
400	2003	0.0751	5.1155e-02	1.11	4.5992e-01	1.13	4.9724e+00	1.05
1600	8003	0.0402	2.3960e-02	1.21	2.1488e-01	1.22	2.4843e+00	1.11

Table 5: Test 1: L^2 , H^1 , and H^2 errors and convergence rates for the convergence test with CSRK-2 time stepping and polynomial order $\ell = 2$ on a Voronoi polygonal grid.

size	dofs	h	L^2 -error	L^2 -eoc	H^1 -error	H^1 -eoc	H^2 -error	H^2 -eoc
25	128	0.3288	1.9833e-01	—	1.7472e+00	—	2.0820e+01	—
100	503	0.1535	4.6127e-02	1.92	4.5037e-01	1.78	9.9688e+00	0.97
400	2003	0.0751	1.0867e-02	2.02	1.0755e-01	2.0	4.9206e+00	0.99
1600	8003	0.0402	2.5869e-03	2.29	2.5990e-02	2.27	2.4679e+00	1.1

Table 6: Test 1: L^2 , H^1 , and H^2 errors and convergence rates for the convergence test with CSRK-2 time stepping and polynomial order $\ell = 4$ on a Voronoi polygonal grid.

size	dofs	h	L^2 -error	L^2 -eoc	H^1 -error	H^1 -eoc	H^2 -error	H^2 -eoc
25	457	0.3288	2.2198e-02	—	1.9974e-01	—	1.9335e+00	—
100	1807	0.1535	5.5609e-03	1.82	5.0147e-02	1.81	4.8954e-01	1.8
400	7207	0.0751	1.0552e-03	2.33	9.7041e-03	2.3	1.0424e-01	2.16
1600	28807	0.0402	1.6145e-04	3.0	1.6223e-03	2.86	2.6661e-02	2.18

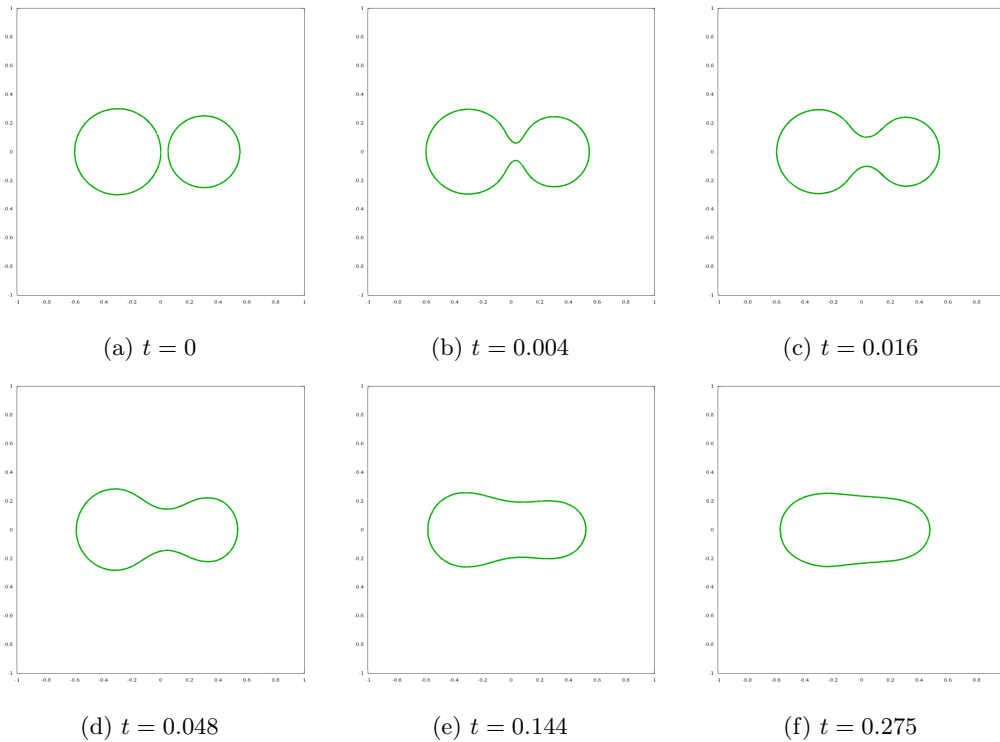


Figure 2: Test 2: Two interacting bubbles. Screenshots of the zero-level sets at times $t = 0, 0.004, 0.016, 0.048, 0.144, 0.3$ with $\varepsilon = 3/100$ are displayed on the 25×25 Voronoi polygonal grid.

5.2 Test 2: Two interacting bubbles

This test is taken from [34, 46] and is dedicated to the evolution of two ellipses. A similar test is investigated in [40]. In particular, we take initial data as follows

$$u_0(x, y) = \tanh\left(\frac{((x - 0.3)^2 + y^2 - 0.25^2)}{\varepsilon}\right) \tanh\left(\frac{((x + 0.3)^2 + y^2 - 0.3^2)}{\varepsilon}\right)$$

where $\tanh(t) = (e^t - e^{-t})/(e^t + e^{-t})$. We monitor the evolution of two ellipses on the domain $\Omega = (-1, 1)^2$ and fix $\ell = 4$, $\varepsilon = 3/100$ for this experiment. We use the CSRK-2 (5.2) time stepping method with $\tau = 10^{-3}$. We show results on the 25×25 Voronoi mesh. The screenshots of the numerical interface at 6 different fixed time frames is shown in Figure 2. Here we see that the initial ellipses evolve and coalesce over time to one ellipse. Note that the observed behaviour and evolution of the interface is in line with the results displayed in [46] for the Morley element.

5.3 Test 3: Evolution of a cross

As considered in e.g. [3, 17, 40], for this experiment we monitor the evolution of initial data relating to a cross-shaped interface between phases. The initial data is described as follows.

$$u_0(x, y) = \begin{cases} 0.95 & \text{if } |(y - \frac{1}{2}) - \frac{2}{5}(x - \frac{1}{2})| + |\frac{2}{5}(x - \frac{1}{2}) + (y - \frac{1}{2})| < \frac{1}{5}, \\ 0.95 & \text{if } |(x - \frac{1}{2}) - \frac{2}{5}(y - \frac{1}{2})| + |\frac{2}{5}(y - \frac{1}{2}) + (x - \frac{1}{2})| < \frac{1}{5}, \\ -0.95 & \text{otherwise.} \end{cases}$$

We carry out this experiment on the unit square using the same two mesh types as in Test 1 (as described in Section 5.1) for three different grid sizes. The grid data for these choices is detailed in Table 7 alongside the total number of dofs for each of these grid sizes. We also take multiple values for the interface parameter: $\varepsilon = 1/100, 1/50$, and $1/25$ and investigate the behaviour of the method for each *fixed* value of epsilon. We also fix $\tau = 10^{-3}$, use the CSRK-2 time stepping method (5.2) for these simulations and run the test to time $T = 0.8$.

Table 7: Combinations of $N \times N$ grids showing the size (total number of polygons), grid size h , and number of dofs for each of the grid choices.

$N \times N$	structured simplex mesh			Voronoi mesh		
	size	h	dofs	size	h	dofs
15×15	450	0.0943	4231	225	0.1008	4057
25×25	1250	0.0566	11551	625	0.0676	11257
45×45	4050	0.0314	36991	2025	0.0373	36457

We only show the evolution of the method for this test on the 25×25 grids for two of the values of interface parameter $\varepsilon = 1/100$ (Figure 3) and $\varepsilon = 1/25$ (Figure 4) at three different fixed time frames. We overlay the grids in the first images in Figures 3 and 4.

Figures 5 and 6 show the evolution at the end time frame ($T = 0.8$) for $\varepsilon = 1/100$ and $\varepsilon = 1/25$, respectively for both the simplex criss mesh and Voronoi mesh. We show the grids overlaid in the first figure, Figure 5. Each figure contains the end time frame for all grid sizes from left to right $15 \times 15, 25 \times 25$, and 45×45 . We can see from Figures 5 and 6 that in all cases the initial data evolves to a circular interface even for the coarse 15×15 grid. Again, for the sake of brevity, we do not show the end evolution for $\varepsilon = 1/50$.

The energy decay for this problem is shown in Figure 7. At each time step we compute the energy $E(u_h)$ (2.2) of the discrete solution u_h . As expected, the energy decreases in nearly all cases. There is a slight increase in the left figure of Figure 7c which corresponds to the interface parameter $\varepsilon = 1/100$ on the coarse 15×15 criss grid, indicating that the interface is unresolved even with the higher order scheme on this grid. We also see in Figures 5 and 6 a slightly larger circular interface on the coarsest grids.

5.4 Test 4: Spinodal decomposition

For this experiment we turn our attention to the spinodal decomposition of a binary mixture. As in [3, 17], to model this phenomenon we choose the initial data u_0 to be a random perturbation between -1 and 1 located in a circle of diameter 0.3 in the centre of the domain and 0 elsewhere. We take the interface parameter to be $\varepsilon = 1/100$, with time step $\tau = 10^{-2}$, and we use the CSRK-2 time stepping method (5.2). Snapshots of the results on both the structured simplex grid and the Voronoi polygonal mesh are shown in Figure 8. Note that the random initial conditions used for the two grids are different and result in the difference in the end configurations seen in Figure 8.

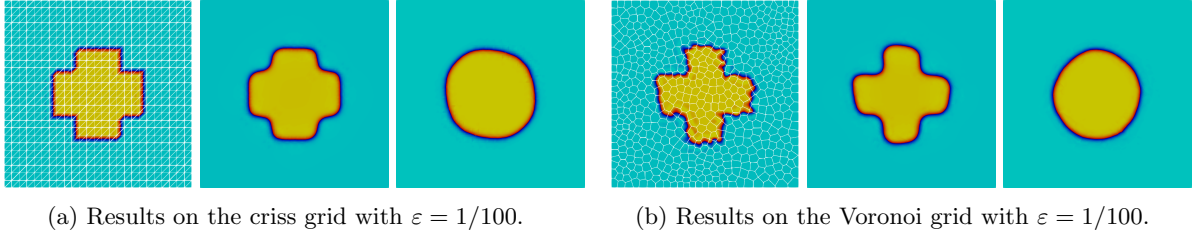


Figure 3: Test 3: evolution of a cross on the 25×25 grids displayed at three different time frames from left to right ($t = 0, 0.004, 0.8$) with $\varepsilon = 1/100$.

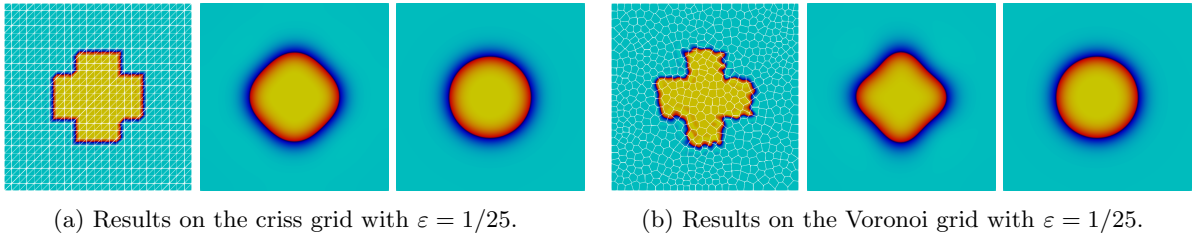


Figure 4: Test 3: evolution of a cross on the 25×25 grids displayed at three different time frames from left to right ($t = 0, 0.004, 0.8$) with $\varepsilon = 1/25$.

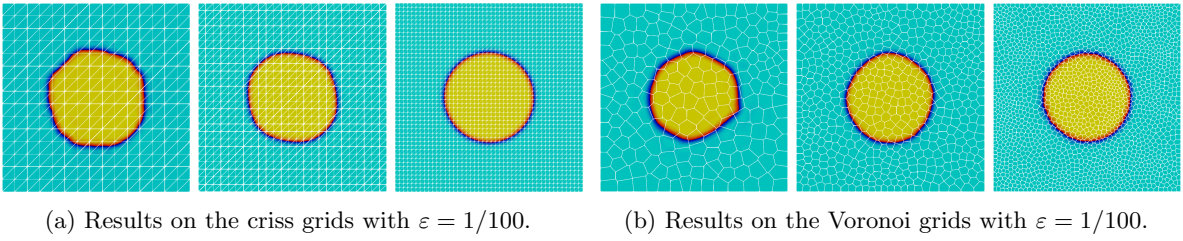


Figure 5: Test 3: evolution of a cross displayed at the end time frame $t = 0.8$ on the grid sizes from left to right 15×15 , 25×25 , and 45×45 with $\varepsilon = 1/100$.

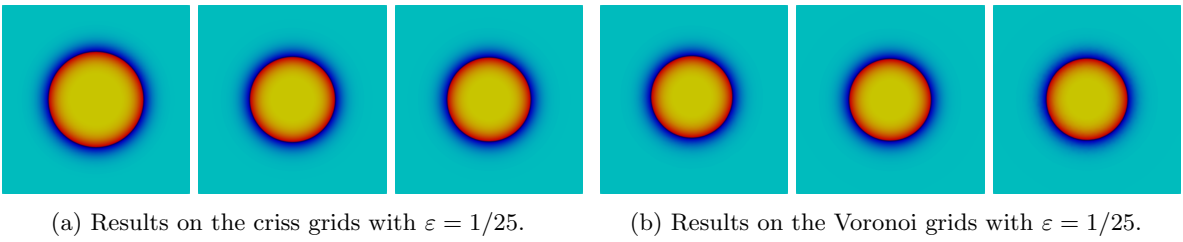
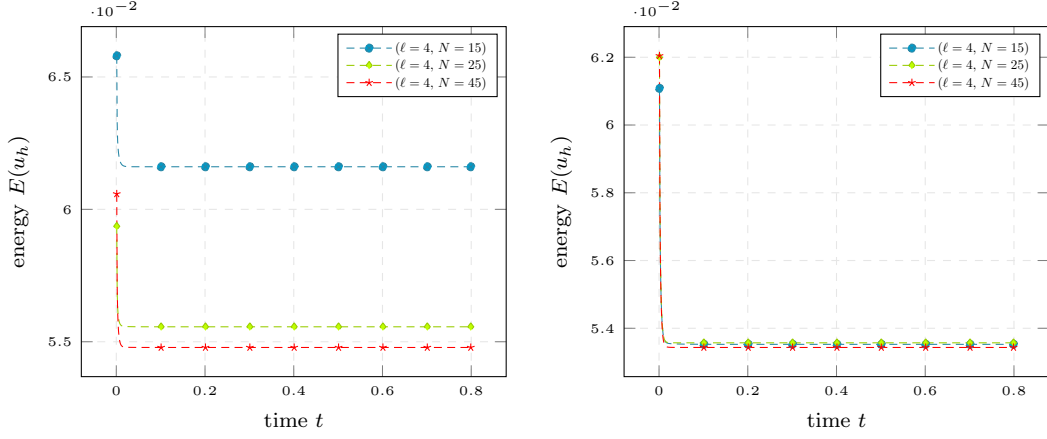
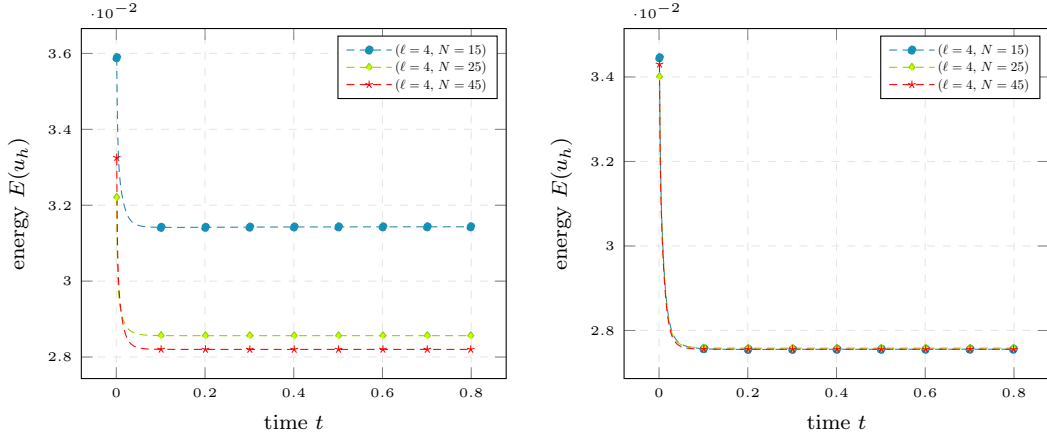


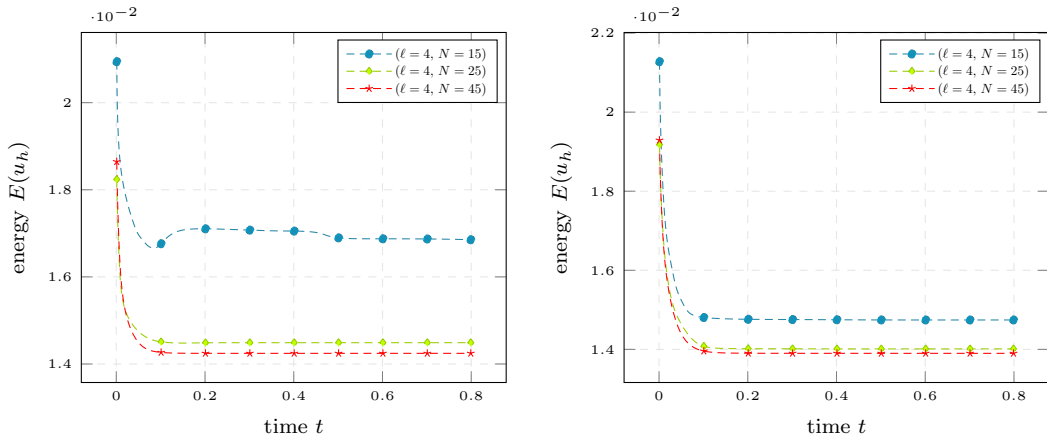
Figure 6: Test 3: evolution of a cross displayed at the end time frame $t = 0.8$ on the grid sizes from left to right 15×15 , 25×25 , and 45×45 with $\varepsilon = 1/25$. The grids used can be seen in Figure 5.



(a) Energy plots for $\varepsilon = 1/25$ on the structured simplex criss mesh (left) and Voronoi polygonal mesh (right).



(b) Energy plots for $\varepsilon = 1/50$ on the structured simplex criss mesh (left) and Voronoi polygonal mesh (right).



(c) Energy plots for $\varepsilon = 1/100$ on the structured simplex criss mesh (left) and Voronoi polygonal mesh (right).

Figure 7: Test 2: energy decay plots (energy $E(u_h)$ vs time t) for the cross evolution problem.

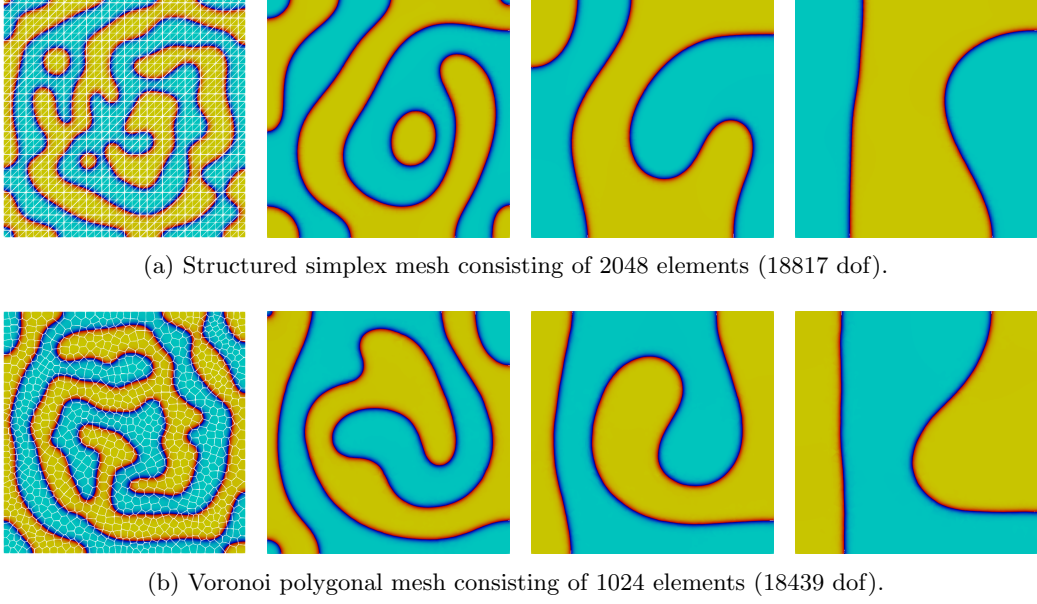


Figure 8: Test 4: spinodal decomposition with order $\ell = 4$ displayed at four time frames from left to right ($t = 0.04, 0.4, 1.6, 5$).

6 Conclusion

In this paper we have developed a fully nonconforming virtual element method of arbitrary approximation order for the discretization of the two dimensional Cahn-Hilliard equation. We applied the projection approach taken in [21] to the fourth-order nonlinear Cahn-Hilliard problem and were able to define the discrete forms directly without using an averaging technique for the nonlinear term, as seen in [3]. This approach enabled us to prove optimal order error estimates in the L^2 -norm for the semidiscrete (continuous-in-time) scheme. We coupled the VEM spatial discretization with a convex splitting Runge-Kutta (CSRK) method to create a fully discrete scheme and the behaviour investigated with numerical experiments. The theoretical convergence result was verified numerically and standard benchmark tests from the literature were carried out.

A Proof of technical results

We dedicate this section to the proof of some technical lemmas necessary for the error analysis. Firstly, we give the proof of Lemma 4.4.

Proof of Lemma 4.4. We begin by introducing the interpolation $I_h z$ of z into our nonconforming VEM space $V_{h,\ell}$,

$$|b(u - P_h u, z)| = |b(u - P_h u, z - I_h z) + b(u - P_h u, I_h z)|.$$

The first term can be bounded easily using the continuity of the bilinear form $b(\cdot, \cdot)$, (4.5), and interpolation properties of I_h (3.6). Hence, we can show that

$$|b(u - P_h u, z - I_h z)| \leq \|u - P_h u\|_{2,h} \|z - I_h z\|_{2,h} \lesssim h^\ell \|u - P_h u\|_{1,h},$$

using (4.5), interpolation properties of z , and (4.10).

We rewrite the remaining term introducing $z_h := I_h z - z$, and see that

$$b(u - P_h u, I_h z) = b(u, z_h) + b(u, z) - b(P_h u, I_h z).$$

We note that the continuous solution u satisfies

$$b(u, z) = \varepsilon^2 a(u, z) + r(u; u, z) + \alpha(u, z) = (\varepsilon^2 \Delta^2 u - \nabla \cdot (\phi'(u) \nabla u) + \alpha u, z).$$

Therefore, using the definition of the elliptic projection in (4.2), it follows that

$$\begin{aligned} b(u, z_h) + b(u, z) &= \varepsilon^2 a(u, z_h) + r(u; u, z_h) + \alpha(u, z_h) + b(u, z) \\ &= (\varepsilon^2 \Delta^2 u - \nabla \cdot (\phi'(u) \nabla u) + \alpha u, z_h + z) + \mathcal{N}(u, z_h) \end{aligned}$$

$$= b_h(P_h u, I_h z) + \mathcal{N}(u, z_h),$$

where $\mathcal{N}(u, z_h)$ is defined in (4.4). Noting that, by definition,

$$b_h(P_h u, I_h z) = b(P_h u, I_h z) + \varepsilon^2 (a_h(P_h u, I_h z) - a(P_h u, I_h z)) + r_h(u; P_h u, I_h z) - r(u; P_h u, I_h z),$$

we observe that

$$\begin{aligned} |b(u - P_h u, I_h z)| &= |b(u, z_h) + b(u, z) - b(P_h u, I_h z) - b_h(P_h u, I_h z) + b_h(P_h u, I_h z)| \\ &\leq |\mathcal{N}(u, z_h)| + \varepsilon^2 |a_h(P_h u, I_h z) - a(P_h u, I_h z)| + |r_h(u; P_h u, I_h z) - r(u; P_h u, I_h z)| \\ &= T_1 + T_2 + T_3. \end{aligned}$$

We now look at each term in turn. For T_1 we apply Lemma 4.2 and (4.10) to see that

$$T_1 \lesssim h^{\ell-1} |z - I_h z|_{2,h} \lesssim h^\ell \|z\|_{3,\Omega} \lesssim h^\ell \|u - P_h u\|_{1,h}. \quad (\text{A.1})$$

For the second term T_2 , we introduce the L^2 projection of z , as well as the L^2 projection of u , and use polynomial consistency from Lemma 3.13. Therefore

$$\begin{aligned} T_2 &= \varepsilon^2 |a_h(P_h u, I_h z) - a(P_h u, I_h z)| \\ &= \varepsilon^2 \left| \sum_{K \in \mathcal{T}_h} a_h^K(I_h z - \mathcal{P}_\ell^K z, P_h u - \mathcal{P}_\ell^K u) - a^K(I_h z - \mathcal{P}_\ell^K z, P_h u - \mathcal{P}_\ell^K u) \right| \\ &\lesssim \varepsilon^2 |I_h z - \mathcal{P}_\ell^K z|_{2,h} |P_h u - \mathcal{P}_\ell^K u|_{2,h} \lesssim h \|z\|_{3,\Omega} h^{\ell-1} \lesssim h^\ell \|u - P_h u\|_{1,h}. \end{aligned} \quad (\text{A.2})$$

For the final term, T_3 , we note that due to the fact that the gradient projection is exact for polynomials, it holds that $r_h(u; \mathcal{P}_\ell^K u, \mathcal{P}_\ell^K z) = r(u; \mathcal{P}_\ell^K u, \mathcal{P}_\ell^K z)$. Therefore,

$$\begin{aligned} T_3 &= |r_h(u; P_h u, I_h z) - r(u; P_h u, I_h z)| \\ &= |r_h(u; P_h u - \mathcal{P}_\ell^K u, I_h z - \mathcal{P}_\ell^K z) + r_h(u; \mathcal{P}_\ell^K u, I_h z) + r_h(u; P_h u, \mathcal{P}_\ell^K z) \\ &\quad - r_h(u; \mathcal{P}_\ell^K u, \mathcal{P}_\ell^K z) + r(u; \mathcal{P}_\ell^K u, \mathcal{P}_\ell^K z) \\ &\quad - r(u; P_h u - \mathcal{P}_\ell^K u, I_h z - \mathcal{P}_\ell^K z) - r(u; \mathcal{P}_\ell^K u, I_h z) - r(u; P_h u, \mathcal{P}_\ell^K z)| \\ &\leq \left| r_h(u; P_h u - \mathcal{P}_\ell^K u, I_h z - \mathcal{P}_\ell^K z) - r(u; P_h u - \mathcal{P}_\ell^K u, I_h z - \mathcal{P}_\ell^K z) \right| \end{aligned} \quad (\text{A.3})$$

$$+ \left| r_h(u; \mathcal{P}_\ell^K u, I_h z) - r(u; \mathcal{P}_\ell^K u, I_h z) \right| \quad (\text{A.4})$$

$$+ \left| r_h(u; P_h u, \mathcal{P}_\ell^K z) - r(u; P_h u, \mathcal{P}_\ell^K z) \right|. \quad (\text{A.5})$$

The first term (A.3) can be treated in the same way as T_2 and we can show that

$$\begin{aligned} &|r_h(u; P_h u - \mathcal{P}_\ell^K u, I_h z - \mathcal{P}_\ell^K z) - r(u; P_h u - \mathcal{P}_\ell^K u, I_h z - \mathcal{P}_\ell^K z)| \\ &\lesssim \|\phi'(u)\|_{L^\infty} |P_h u - \mathcal{P}_\ell^K u|_{1,h} |I_h z - \mathcal{P}_\ell^K z|_{1,h} \lesssim h^\ell \|u - P_h u\|_{1,h}. \end{aligned} \quad (\text{A.6})$$

For the next term (A.4), since $\mathcal{P}_\ell^K u \in \mathbb{P}_\ell(K)$, the stabilization part of r_h vanishes and so we have the following

$$\begin{aligned} \left| r_h(u; \mathcal{P}_\ell^K u, I_h z) - r(u; \mathcal{P}_\ell^K u, I_h z) \right| &= \left| \sum_{K \in \mathcal{T}_h} \int_K \phi'(u) (\mathcal{P}_{\ell-1}^K (\nabla \mathcal{P}_\ell^K u) \cdot \mathcal{P}_{\ell-1}^K \nabla I_h z - \nabla \mathcal{P}_\ell^K u \cdot \nabla I_h z) \, dx \right| \\ &= \left| \sum_{K \in \mathcal{T}_h} \int_K \phi'(u) (\nabla \mathcal{P}_\ell^K u) \cdot (\mathcal{P}_{\ell-1}^K - I) \nabla I_h z \, dx \right| \\ &= \left| \sum_{K \in \mathcal{T}_h} \int_K (\mathcal{P}_{\ell-1}^K - I) (\phi'(u) \nabla \mathcal{P}_\ell^K u) \cdot (\nabla I_h z - \mathcal{P}_0^K \nabla z) \, dx \right| \\ &\leq \sum_{K \in \mathcal{T}_h} \|(\mathcal{P}_{\ell-1}^K - I) \phi'(u) \nabla \mathcal{P}_\ell^K u\|_{0,K} \|\nabla I_h z - \mathcal{P}_0^K \nabla z\|_{0,K} \\ &\lesssim h^{\ell-1} h \|z\|_{3,\Omega} \lesssim h^\ell \|u - P_h u\|_{1,h}. \end{aligned} \quad (\text{A.7})$$

For the final term in T_3 , (A.5), we again note that since $\mathcal{P}_\ell^K z \in \mathbb{P}_\ell(K)$, the stabilization part of r_h vanishes, and so

$$\left| r_h(u; P_h u, \mathcal{P}_\ell^K z) - r(u; P_h u, \mathcal{P}_\ell^K z) \right| = \left| \sum_{K \in \mathcal{T}_h} \int_K \phi'(u) (\mathcal{P}_{\ell-1}^K \nabla P_h u \cdot \mathcal{P}_{\ell-1}^K \nabla \mathcal{P}_\ell^K z - \nabla P_h u \cdot \mathcal{P}_\ell^K z) \, dx \right|$$

$$\begin{aligned}
&= \left| \sum_{K \in \mathcal{T}_h} \int_K \phi'(u) (\mathcal{P}_{\ell-1}^K - I) \nabla P_h u \cdot (\nabla \mathcal{P}_\ell^K z) \, dx \right| \\
&= \left| \sum_{K \in \mathcal{T}_h} \int_K \phi'(u) ((I - \mathcal{P}_{\ell-1}^K)(\nabla u - \nabla P_h u) - (I - \mathcal{P}_{\ell-1}^K) \nabla u) \cdot (\nabla \mathcal{P}_\ell^K z) \, dx \right| \\
&\leq \sum_{K \in \mathcal{T}_h} \|\phi'(u)\|_{L^\infty} h^1 |\nabla u - \nabla P_h u|_{1,K} \|\nabla \mathcal{P}_\ell^K z\|_{0,K} \\
&\quad + \sum_{K \in \mathcal{T}_h} \|\phi'(u)\|_{L^\infty} h^{\ell-1+1} |\nabla u|_{\ell,K} \|\nabla \mathcal{P}_\ell^K z\|_{0,K} \\
&\lesssim h^\ell \|u - P_h u\|_{1,h},
\end{aligned} \tag{A.8}$$

where we have used (4.5), (4.10), and stability of the L^2 projection in the last step. Hence, by combining the estimates from (A.1), (A.2), (A.6), (A.7), and (A.8), it holds that

$$|b(u - P_h u, I_h z)| \leq T_1 + T_2 + T_3 \lesssim h^\ell \|u - P_h u\|_{1,h}.$$

This concludes the proof. \square

Next, we give the proof of Lemma 4.5, necessary for the proof of the estimates (4.7)-(4.8) in Lemma 4.3.

Proof of Lemma 4.5. Using Lemma 3.9, since $P_h u, \eta_h \in V_{h,\ell}$, we can show the following

$$\begin{aligned}
&|(\phi''(u) u_t \Pi_1^K P_h u, \Pi_1^K \eta_h)_{0,h} - (\phi''(u) u_t \nabla u, \nabla \eta_h)_{0,h}| \\
&= \left| \sum_{K \in \mathcal{T}_h} \int_K \phi''(u) u_t (\mathcal{P}_{\ell-1}^K \nabla P_h u \cdot \mathcal{P}_{\ell-1}^K \nabla \eta_h - \nabla u \cdot \nabla \eta_h) \, dx \right| \\
&= \left| \sum_{K \in \mathcal{T}_h} \int_K \left(\mathcal{P}_{\ell-1}^K (\phi''(u) u_t \mathcal{P}_{\ell-1}^K \nabla P_h u) - \phi''(u) u_t \nabla u \right) \cdot \nabla \eta_h \, dx \right|.
\end{aligned}$$

We now introduce the constant projection of the gradient of η_h , $\mathcal{P}_0^K(\nabla \eta_h)$ and see that

$$\begin{aligned}
&|(\phi''(u) u_t \Pi_1^K P_h u, \Pi_1^K \eta_h)_{0,h} - (\phi''(u) u_t \nabla u, \nabla \eta_h)_{0,h}| \\
&\leq \left| \sum_{K \in \mathcal{T}_h} \int_K \left(\mathcal{P}_{\ell-1}^K \{ \phi''(u) u_t \mathcal{P}_{\ell-1}^K \nabla P_h u - \phi''(u) u_t \mathcal{P}_{\ell-1}^K \nabla u \} \right) \cdot \nabla \eta_h \, dx \right| \\
&\quad + \left| \sum_{K \in \mathcal{T}_h} \int_K \left((\mathcal{P}_{\ell-1}^K - I) (\phi''(u) u_t \mathcal{P}_{\ell-1}^K \nabla u) \right) \cdot (\nabla \eta_h - \mathcal{P}_0^K(\nabla \eta_h)) \, dx \right| \\
&\quad + \left| \sum_{K \in \mathcal{T}_h} \int_K \left(\phi''(u) u_t \mathcal{P}_{\ell-1}^K \nabla u - \phi''(u) u_t \nabla u \right) \cdot \nabla \eta_h \, dx \right| \\
&\leq \sum_{K \in \mathcal{T}_h} \|\phi''(u) u_t \mathcal{P}_{\ell-1}^K (\nabla P_h u - \nabla u)\|_{0,K} \|\nabla \eta_h\|_{0,K} \\
&\quad + \sum_{K \in \mathcal{T}_h} h^{\ell-1} |\phi''(u) u_t \mathcal{P}_{\ell-1}^K \nabla u|_{\ell-1} \|\nabla \eta_h - \mathcal{P}_0^K(\nabla \eta_h)\|_{0,K} \\
&\quad + \sum_{K \in \mathcal{T}_h} \|\phi''(u) u_t\|_{L^\infty} \|\mathcal{P}_{\ell-1}^K \nabla u - \nabla u\|_{0,K} \|\nabla \eta_h\|_{0,K} \\
&\lesssim h^\ell \|\eta_h\|_{2,h},
\end{aligned}$$

where we have used stability of the L^2 projection and (4.6). \square

Lastly, we give the proof of Lemma 4.8, which is necessary for the proof of L^2 convergence in Theorem 4.9.

Proof of Lemma 4.8. Recall that for any $w_h \in V_{h,\ell} \subset H_\ell^{2,nc}(\mathcal{T}_h)$, and for any edge $e \in \mathcal{E}_h$, the following properties hold,

$$\int_e [w_h] p \, ds = 0 \quad \forall p \in \mathbb{P}_{\ell-3}(e), \tag{A.9}$$

$$\int_e [\partial_n w_h] p \, ds = 0 \quad \forall p \in \mathbb{P}_{\ell-2}(e). \tag{A.10}$$

Observe that the following holds

$$\left| \sum_{K \in \mathcal{T}_h} \int_{\partial K} (\partial_n z_h) w_h \, ds \right| = \left| \sum_{e \in \mathcal{E}_h} \int_e (\{w_h\} [\partial_n z_h] + \{\partial_n z_h\} [w_h]) \, ds \right| \leq A_I + A_{II}$$

where we use $\{\cdot\}$ to denote the average of a function v , $\{v\} := \frac{1}{2}(v|_{K^+} + v|_{K^-})$ for any interior edge $e \subset \partial K^+ \cap \partial K^-$. For a boundary edge $e \in \mathcal{E}_h^{\text{bdry}}$ we define $\{v\} := v|_e$.

Using (A.10), for the first term A_I , it holds that

$$\begin{aligned} A_I &= \left| \sum_{e \in \mathcal{E}_h} \int_e \{w_h\} [\partial_n z_h] \, ds \right| \leq \left| \sum_{e \in \mathcal{E}_h} \int_e (\{w_h\} - \mathcal{P}_0^e \{w_h\}) [\partial_n z_h] \, ds \right| \\ &\leq \left| \sum_{e \in \mathcal{E}_h} \int_e (\{w_h\} - \mathcal{P}_0^e \{w_h\}) ([\partial_n z_h] - \mathcal{P}_0^e [\partial_n z_h]) \, ds \right| \\ &\lesssim h^{1-\frac{1}{2}} |w_h|_{1,h} h^{1-\frac{1}{2}} |z_h|_{2,h} \\ &\lesssim h |w_h|_{1,h} |z_h|_{2,h}. \end{aligned}$$

For the second term A_{II} , we follow the method used in [4]. In view of Remark 2.3, for each edge we define the linear Lagrange interpolant $I_{T(e)}^1$ of z_h on the sub-triangle $T(e)$, made from connecting the interior point x_K to the endpoints of the edge e . Since $z_h \in V_{h,\ell}$, it also satisfies $z_h \in H^2(K)$, and so we can build the interpolant by using the values at the vertices of $T(e)$. Further, z_h is continuous at the endpoints of e and so

$$[I_{T(e)}^1(w_h)]|_e = 0.$$

Therefore, by using standard interpolation estimates and a trace inequality, we see that

$$A_{II} = \left| \sum_{e \in \mathcal{E}_h} \int_e \{\partial_n z_h\} [w_h] \, ds \right| = \left| \sum_{e \in \mathcal{E}_h} \int_e \{\partial_n z_h\} ([w_h] - [I_{T(e)}^1(w_h)]) \, ds \right| \lesssim h |z_h|_{2,h} |w_h|_{2,h},$$

hence (4.18) holds, as required. \square

Acknowledgements

The authors would like to acknowledge the University of Warwick Scientific Computing Research Technology Platform for assistance in the research described in this paper.

References

- [1] AHMAD, B., ALSAEDI, A., BREZZI, F., MARINI, L. D., AND RUSSO, A. Equivalent projectors for virtual element methods. *Comput. Math. Appl.* 66, 3 (2013), 376–391.
- [2] ALNÆS, M. S., LOGG, A., ØLGAARD, K. B., ROGNES, M. E., AND WELLS, G. N. Unified form language: A domain-specific language for weak formulations of partial differential equations. *ACM Trans. Math. Softw.* 40, 2 (2014).
- [3] ANTONIETTI, P. F., BEIRÃO DA VEIGA, L., SCACCHI, S., AND VERANI, M. A C^1 virtual element method for the Cahn–Hilliard equation with polygonal meshes. *SIAM J. Numer. Anal.* 54, 1 (2016), 34–56.
- [4] ANTONIETTI, P. F., MANZINI, G., AND VERANI, M. The fully nonconforming virtual element method for biharmonic problems. *Math. Models Methods Appl. Sci.* 28, 02 (2018), 387–407.
- [5] ANTONIETTI, P. F., MANZINI, G., AND VERANI, M. The conforming virtual element method for polyharmonic problems. *Comput. Math. Appl.* 79, 7 (2020), 2021–2034.
- [6] ANTONIETTI, P. F., SCACCHI, S., VACCA, G., AND VERANI, M. C^1 -VEM for some variants of the Cahn–Hilliard equation: a numerical exploration. *Discrete Contin. Dyn. Syst. Ser. S* 15 (2022).
- [7] BASTIAN, P., BLATT, M., DEDNER, A., ENGWER, C., KLÖFKORN, R., KORNUBER, R., OHLBERGER, M., AND SANDER, O. A generic grid interface for parallel and adaptive scientific computing. part II: Implementation and tests in DUNE. *Computing* 82, 2–3 (2008), 121–138.
- [8] BEIRÃO DA VEIGA, L., BREZZI, F., CANGIANI, A., MANZINI, G., MARINI, L. D., AND RUSSO, A. Basic principles of virtual element methods. *Math. Models Methods Appl. Sci.* 23, 01 (2013), 199–214.
- [9] BEIRÃO DA VEIGA, L., LOVADINA, C., AND RUSSO, A. Stability analysis for the virtual element method. *Math. Models Methods Appl. Sci.* 27, 13 (2017), 2557–2594.

- [10] BEIRÃO DA VEIGA, L., LOVADINA, C., AND VACCA, G. Divergence free virtual elements for the Stokes problem on polygonal meshes. *ESAIM Math. Model. Numer. Anal.* 51, 2 (2015), 509–535.
- [11] BEIRÃO DA VEIGA, L., AND MANZINI, G. A virtual element method with arbitrary regularity. *IMA J. Numer. Anal.* 34, 2 (2014), 759–781.
- [12] BRENNER, S. C., AND SCOTT, L. R. *The mathematical theory of finite element methods*, 3rd ed. No. 15 in Texts in applied mathematics. Springer, New York, NY, 2008.
- [13] BRENNER, S. C., AND SUNG, L.-Y. Virtual element methods on meshes with small edges or faces. *Math. Models Methods Appl. Sci.* 28, 07 (2018), 1291–1336.
- [14] CAHN, J. W. On spinodal decomposition. *Acta metallurgica* 9, 9 (1961), 795–801.
- [15] CAHN, J. W., AND HILLIARD, J. E. Free energy of a nonuniform system. I. Interfacial free energy. *The Journal of chemical physics* 28, 2 (1958), 258–267.
- [16] CANGIANI, A., MANZINI, G., AND SUTTON, O. J. Conforming and nonconforming virtual element methods for elliptic problems. *IMA J. Numer. Anal.* 37, 3 (2017), 1317–1354.
- [17] CHAVE, F., DI PIETRO, D. A., MARCHE, F., AND PIGEONNEAU, F. A hybrid high-order method for the Cahn–Hilliard problem in mixed form. *SIAM J. Numer. Anal.* 54, 3 (2016), 1873–1898.
- [18] CHOO, S., AND LEE, Y. A discontinuous galerkin method for the Cahn-Hilliard equation. *J. Appl. Math. Comput.* 18, 1-2 (2005), 113–126.
- [19] CROUZEIX, M., AND THOMÉE, V. The stability in L_p and W^1_p of the L_2 projection onto finite element function spaces. *Math. Comp.* 48, 178 (1987), 521–532.
- [20] DEDNER, A., AND HODSON, A. A framework for implementing general virtual element spaces. *arXiv preprint arXiv:2208.08978* (2022).
- [21] DEDNER, A., AND HODSON, A. Robust nonconforming virtual element methods for general fourth-order problems with varying coefficients. *IMA J. Numer. Anal.* 42, 2 (2022), 1364–1399.
- [22] DEDNER, A., KLOEFKORN, R., AND NOLTE, M. Python bindings for the DUNE-FEM module. *Zenodo* 10 (2020).
- [23] DEDNER, A., KLÖFKORN, R., NOLTE, M., AND OHLBERGER, M. A generic interface for parallel and adaptive discretization schemes: abstraction principles and the DUNE-FEM module. *Computing* 90, 3-4 (2010), 165–196.
- [24] DEDNER, A., AND NOLTE, M. The Dune Python module. *arXiv preprint arXiv:1807.05252* (2018).
- [25] DI PIETRO, D. A., AND ERN, A. A hybrid high-order locking-free method for linear elasticity on general meshes. *Comput. Methods Appl. Mech. Engrg.* 283 (2015), 1–21.
- [26] DOLCETTA, I. C., VITA, S. F., AND MARCH, R. Area-preserving curve-shortening flows: from phase separation to image processing. *Interfaces Free Bound.* 4, 4 (2002), 325–343.
- [27] ELLIOTT, C. M. The Cahn-Hilliard model for the kinetics of phase separation. *Mathematical models for phase change problems* (1989), 35–73.
- [28] ELLIOTT, C. M., AND FRENCH, D. A. Numerical studies of the Cahn-Hilliard equation for phase separation. *IMA J. Appl. Math.* 38, 2 (1987), 97–128.
- [29] ELLIOTT, C. M., AND FRENCH, D. A. A nonconforming finite-element method for the two-dimensional Cahn–Hilliard equation. *SIAM J. Numer. Anal.* 26, 4 (1989), 884–903.
- [30] ELLIOTT, C. M., FRENCH, D. A., AND MILNER, F. A second order splitting method for the Cahn-Hilliard equation. *Numer. Math.* 54, 5 (1989), 575–590.
- [31] ELLIOTT, C. M., AND SONGMU, Z. On the Cahn-Hilliard equation. *Arch. Ration. Mech. Anal.* 96, 4 (1986), 339–357.
- [32] ELLIOTT, C. M., AND STUART, A. The global dynamics of discrete semilinear parabolic equations. *SIAM J. Numer. Anal.* 30, 6 (1993), 1622–1663.
- [33] EYRE, D. J. Unconditionally gradient stable time marching the Cahn-Hilliard equation. *MRS Online Proceedings Library (OPL)* 529 (1998).
- [34] FENG, X., AND WU, H. A posteriori error estimates for finite element approximations of the Cahn-Hilliard equation and the Hele-Shaw flow. *J. Comput. Math.* (2008), 767–796.
- [35] GÓMEZ, H., CALO, V. M., BAZILEVS, Y., AND HUGHES, T. J. Isogeometric analysis of the Cahn–Hilliard phase-field model. *Comput. Methods Appl. Mech. Engrg.* 197, 49-50 (2008), 4333–4352.
- [36] KÄSTNER, M., METSCH, P., AND DE BORST, R. Isogeometric analysis of the Cahn–Hilliard equation—a convergence study. *J. Comput. Phys.* 305 (2016), 360–371.
- [37] KAY, D., STYLES, V., AND SÜLI, E. Discontinuous galerkin finite element approximation of the Cahn–Hilliard equation with convection. *SIAM J. Numer. Anal.* 47, 4 (2009), 2660–2685.

- [38] LEE, H. G. Stability condition of the Second-Order SSP-IMEX-RK method for the Cahn–Hilliard equation. *Mathematics* 8, 1 (2020), 11.
- [39] LIU, X., AND CHEN, Z. A virtual element method for the Cahn–Hilliard problem in mixed form. *Appl. Math. Lett.* 87 (2019), 115–124.
- [40] LIU, X., HE, Z., AND CHEN, Z. A fully discrete virtual element scheme for the Cahn–Hilliard equation in mixed form. *Comput. Phys. Commun.* 246 (2020), 106870.
- [41] MASCOTTO, L., PERUGIA, I., AND PICHLER, A. Non-conforming harmonic virtual element method: h - and p -versions. *J. Sci. Comput.* 77, 3 (2018), 1874–1908.
- [42] MORA, D., RIVERA, G., AND RODRÍGUEZ, R. A virtual element method for the Steklov eigenvalue problem. *Math. Models Methods Appl. Sci.* 25, 08 (2015), 1421–1445.
- [43] SHIN, J., LEE, H. G., AND LEE, J.-Y. Unconditionally stable methods for gradient flow using Convex Splitting Runge–Kutta scheme. *J. Comput. Phys.* 347 (2017), 367–381.
- [44] THOMÉE, V. *Galerkin finite element methods for parabolic problems*, vol. 25. Springer Science & Business Media, 2007.
- [45] WELLS, G. N., KUHL, E., AND GARIKIPATI, K. A discontinuous galerkin method for the Cahn–Hilliard equation. *J. Comput. Phys.* 218, 2 (2006), 860–877.
- [46] WU, S., AND LI, Y. Analysis of the Morley element for the Cahn–Hilliard equation and the Hele–Shaw flow. *ESAIM Math. Model. Numer. Anal.* 54, 3 (2020), 1025–1052.
- [47] ZHANG, S., AND WANG, M. A nonconforming finite element method for the Cahn–Hilliard equation. *J. Comput. Phys.* 229, 19 (2010), 7361–7372.
- [48] ZHAO, J., ZHANG, B., CHEN, S., AND MAO, S. The Morley-type virtual element for plate bending problems. *J. Sci. Comput.* 76, 1 (2018), 610–629.
- [49] ZHAO, J., ZHANG, B., AND ZHU, X. The nonconforming virtual element method for parabolic problems. *Appl. Numer. Math.* 143 (2019), 97–111.